Involvement of CFTR in the pathogenesis of pulmonary arterial hypertension

Hélène Le Ribeuz, Lucie To, Maria-Rosa Ghigna, Clémence Martin, Chandran Nagaraj, Elise Dreano, Catherine Rucker-Martin, Barbara Girerd, Christine Pechoux, Mélanie Lambert, et al.

EUROPEAN RESPIRATORY *journal*

FLAGSHIP SCIENTIFIC JOURNAL OF ERS

Early View

Original article

Involvement of CFTR in the pathogenesis of pulmonary arterial hypertension

Hélène Le Ribeuz, Lucie To, Maria-Rosa Ghigna, Clémence Martin, Chandran Nagaraj, Elise Dreano, Catherine Rucker-Martin, Barbara Girerd, Jérôme Bouliguan, Christine Pechoux, Mélanie Lambert, Angèle Boet, Justin Issard, Olaf Mercier, Konrad Hoetzenecker, Boris Manoury, Frédéric Becq, Pierre-Régis Burgel, Charles-Henry Cottart, Andrea Olschewski, Isabelle Sermet-Gaudelus, Frédéric Perros, Marc Humbert, David Montani, Fabrice Antigny

Please cite this article as: Le Ribeuz H, To L, Ghigna M-R, *et al*. Involvement of CFTR in the pathogenesis of pulmonary arterial hypertension. *Eur Respir J* 2021; in press (https://doi.org/10.1183/13993003.00653-2020).

Involvement of CFTR in the pathogenesis of pulmonary arterial hypertension

Hélène Le Ribeuz[1,2,3], Lucie To[1,2,3], Maria-Rosa Ghigna[1,2,3], Clémence Martin[4,5], Chandran Nagaraj[6], Elise Dreano[7] Catherine Rucker-Martin[1,2,3], Barbara Girerd[1,2,3], Jérôme Bouliguan[8], Christine Pechoux[9], Mélanie Lambert[1,2,3], Angèle Boet[1,2,3], Justin Issard[1,2,3], Olaf Mercier[1,2,3], Konrad Hoetzenecker[10], Boris Manoury[11], Frédéric Becq[12], Pierre-Régis Burgel[4, 5], Charles-Henry Cottart[7], Andrea Olschewski[5,13] Isabelle Sermet-Gaudelus[7], Frédéric Perros[1,2,3], Marc Humbert[1,2,3], David Montani[1,2,3] and Fabrice Antigny[1,2,3]

Affiliations

[1]*Université Paris-Saclay, Faculté de Médecine, Le Kremlin-Bicêtre, France (H. L.-R., L. T., M.-R. G., C. R.-M., B. G., J. B., M. L., A. B., O. M., F. P., D. M., M. H., F. A.)*

[2]*INSERM UMR_S 999 « Hypertension pulmonaire: Physiopathologie et Innovation Thérapeutique », Hôpital Marie Lannelongue, Le Plessis-Robinson, France (H. L.-R., L. T., M.-R. G., C. R.-M., B. G., M. L., A. B., O. M., F. P., D. M., M. H., F. A.)*

[3]*Assistance Publique – Hôpitaux de Paris (AP-HP), Service de Pneumologie et Soins Intensifs Respiratoires, Centre de Référence de l'Hypertension Pulmonaire, Hôpital Bicêtre, Le Kremlin-Bicêtre, France. (H. L.-R., L. T., M.-R. G., C. R.-M., B. G., M. L., A. B., O. M., F. P., D. M., M. H., F. A.)*

[4] *Assistance Publique – Hôpitaux de Paris (AP-HP), Dept of Respiratory Medicine, Centre de Référence Maladie Rare Mucoviscidose, ERN-Lung, Cochin Hospital, 27 rue du Faubourg Saint Jacques, 75014 Paris, France (C. M., P.-R. B.)*

[5] *Inserm U1016, Institut Cochin, Université de Paris, Paris, France (C. M., P.-R. B.)*

[6] *Ludwig Boltzmann Institute for Lung Vascular Research, Graz, Austria (C. N., A. O.)*

[7] *Inserm U1151 – CNRS UMR 8253 – Institut Necker Enfants Malades, Centre Maladie Rare Mucoviscidose, ERN Lung, Université de Paris, Paris, France (E. D., C.-H. C., I. S.-G.)*

[8] *Laboratoire de Génétique Moléculaire, Pharmacogénétique et Hormonologie, Assistance Publique-Hôpitaux de Paris (AP-HP), Hôpital Bicêtre, Le Kremlin-Bicêtre, France; INSERM UMR-1185, Université Paris Saclay, Faculté de Médecine, Le Kremlin Bicêtre, France (J. B).*

[9] *GABI, INRA, AgroParisTech, Université Paris-Saclay, 78350 Jouy-en-Josas, France (C. P.)*

[10] *Department of Thoracic Surgery, Medical University of Vienna, Vienna, Austria (K.H.)*

[11] *Signalisation et Physiopathologie Cardiovasculaire – UMR_S 1180, Univ. Paris-Sud, INSERM, Université Paris-Saclay, Châtenay-Malabry, France (B. M.)*

[12] *Laboratoire Signalisation et Transports Ioniques Membranaires, Université de Poitiers, 86073 Poitiers Cedex 9, France (F. B.)*

[13] *Experimental Anesthesiology, Department of Anesthesiology and Intensive Care Medicine, Medical University of Graz, Graz, Austria (A. O.).*

Corresponding author

Fabrice Antigny, INSERM UMR_S 999, Hôpital Marie Lannelongue, 133, Avenue de la Résistance, F-92350 Le Plessis Robinson, France. Fax: (33) 1 40 94 25 22, Tel.: (33) 1 40 94 22 99, E-mail: fabrice.antigny@universite-paris-sacaly.fr

Tweetable abstract @ERSpublications

CFTR expression is lost in the pulmonary arteries of human pulmonary arterial hypertension (PAH) patients and experimental PAH models. We found that pharmacological inhibition of CFTR increases vascular cell proliferation and reduces pulmonary artery relaxation, contributing to PAH pathogenesis.

Keywords: CFTR, pulmonary arterial hypertension, relaxation, hypoxia, monocrotaline

Word count: 4490

Figures: 8

ABSTRACT

Introduction- A reduction in pulmonary artery (PA) relaxation is a key event in pulmonary arterial hypertension (PAH) pathogenesis. CFTR dysfunction in airway epithelial cells plays a central role in cystic fibrosis (CF); CFTR is also expressed in PAs and has been shown to control endothelium-independent relaxation.

Aim and objectives- We aimed to delineate the role of CFTR in PAH pathogenesis through observational and interventional experiments in human tissues and animal models.

Methods and results- RT-Q-PCR, confocal imaging and electron microscopy showed that CFTR expression was reduced in PAs from patients with idiopathic PAH (iPAH) and in rats with monocrotaline-induced pulmonary hypertension (PH). Moreover, using myograph on human, pig and rat PAs, we demonstrated that CFTR activation induces PAs relaxation. CFTR-mediated PA relaxation was reduced in PAs from iPAH patients and rats with monocrotaline- or chronic hypoxia-induced PH. Long-term *in vivo* CFTR inhibition in rats significantly increased right ventricular systolic pressure, which was related to exaggerated pulmonary vascular cell proliferation *in situ* and vessel neomuscularization. Pathologic assessment of lungs from patients with severe CF (*F508del-CFTR*) revealed severe PA remodeling with intimal fibrosis and medial hypertrophy. Lungs from homozygous *F508delCftr* rats exhibited pulmonary vessel neomuscularization. The elevations in right ventricular systolic pressure and end diastolic pressure in monocrotaline-exposed rats with chronic CFTR inhibition were more prominent than those in vehicle-exposed rats.

Conclusions- CFTR expression is strongly decreased in PA smooth muscle and endothelial cells in human and animal models of PH. CFTR inhibition increases vascular cell proliferation and strongly reduces PA relaxation.

INTRODUCTION

Pulmonary arterial hypertension (PAH) is a progressive and severe disease with an estimated prevalence of 15 to 50 per million people in the population[1]. When no causative factors are identified, PAH is termed idiopathic PAH (iPAH). However, it can also be heritable; induced by drugs or toxins; or associated with other conditions, such as connective tissue disease, congenital heart disease, portal hypertension, and HIV infection[2]. In the new pulmonary hypertension (PH) classification proposed during the 6th PH World Symposium in 2018, PH is hemodynamically defined by a mean pulmonary artery (PA) pressure (mPAP) >20 mmHg and a pulmonary vascular resistance (PVR) >3 Wood units at rest[1]. PH is the consequence of an increase in pulmonary vascular resistance due to remodeling of distal PAs and arterioles (diameter <500 μm) that causes adaptive right ventricular (RV) hypertrophy and, when unchecked, right heart failure[3]. PA remodeling is characterized mainly by an increase in PA vasoconstriction, a reduction in PA relaxation and an imbalance between pulmonary vascular cell proliferation and apoptosis in favor of cell proliferation and apoptosis resistance[2]. Remodeling of ion channels in several families contributes to the pathogenesis of PAH, including Cl^- channels[4]. Pulmonary arterial smooth muscle cells (PASMCs) have been described to exhibit various Cl^- currents, including voltage-sensitive, volume-regulated, Ca^{2+}-activated and cystic fibrosis transmembrane conductance regulator (CFTR)-mediated Cl^- currents[4]. The Ca^{2+}-activated Cl^- channel isoform TMEM16A was recently found to be upregulated in PASMCs from iPAH patients, contributing to vasoconstriction and remodeling of PAs in PAH. Papp et al also demonstrated that *CFTR* mRNA levels are severely reduced in PAs isolated from iPAH patients and that pharmacological inhibition of TMEM16A may be a novel therapeutic approach to reduce PA remodeling in PAH[5]. The CFTR channel is a cyclic adenosine monophosphate (cAMP)-dependent and ATP-gated Cl^- channel expressed at the apical membrane in epithelial cells, and mutations in the *CFTR* gene are responsible for cystic fibrosis (CF)[6]. CFTR is expressed not only in epithelial cells but also in different cell types, including cardiac muscle, endothelial, tracheal smooth muscle and vascular smooth muscle cells[7].

Robert et al demonstrated that CFTR is also expressed in rat PAs and contributes to endothelium-independent relaxation of PAs[8]. More recently, Totani et al. demonstrated that CFTR is functionally

expressed in human pulmonary arterial endothelial cells (PAECs)[9]. PH is a recognized comorbidity associated with mortality in CF patients[10–12]. The prevalence of PH in CF is largely unknown, but in some cohorts, such as the Florida CF cohort, approximately 60% of CF patients developed PH[13]. Wells et al. found that PA enlargement, measured by computed tomography, is present in approximately half of CF patients and is associated with a risk of pulmonary exacerbation[11].

However, the role of CFTR dysfunction in the remodeled pulmonary vascular bed has not yet been investigated. In the present study, we first investigated the expression of CFTR in patients with iPAH. We also evaluated the role of CFTR in the development of PH using well-established PH rat models induced by monocrotaline (MCT) or chronic hypoxia (CH) exposure. Using organ bath studies, we measured the involvement of CFTR in PA relaxation in humans, pigs and rats. Furthermore, we analyzed the consequences of chronic long-term *in vivo* inhibition of CFTR in rats using a selective CFTR inhibitor ($CFTR_{inh172}$) at the pulmonary vascular level. Finally, we histologically analyzed PAs from CF patients and *F508delCftr* homozygous rats. Our overall hypothesis is that loss of function of CFTR in PAH contributes to PAH pathogenesis.

MATERIALS AND METHODS

A detailed description of the Materials and Methods is presented in the Online Data Supplement.

RESULTS

Reduced expression of CFTR in PAs from PAH patients

We analyzed the localization of CFTR via immunohistochemistry of paraffin-embedded lung sections from control and iPAH patients (Figure 1). In both control and iPAH patients, CFTR staining labeled PAECs and PASMCs (red arrow), but the staining intensity was lower in pulmonary vascular cells from iPAH patients than in those from control patients (red arrow) (Figure 1i). CFTR staining was reduced within plexiform lesions, the characteristic morphological hallmarks of advanced PAH (Figure 1ii and iii), but the staining intensity was less affected in PAs from patients with PH associated with COPD (Group 3 PH) (Figure 1iv).

CFTR staining confirmed that the protein localized at the apical membranes of airway epithelial cells in control iPAH patients without variations in fluorescence intensity (not shown). Next, we analyzed the expression of CFTR by immunofluorescence staining in frozen lung sections of control and iPAH patients. In PAs from controls, CFTR staining (red) was localized in both PAECs (blue arrow) and PASMCs (blue square) (Figure 2A). Conversely, CFTR staining seemed to be reduced in PAECs and PASMCs in iPAH PAs. Immunofluorescence staining for CFTR in bronchi demonstrated clear CFTR staining at the apical membranes of airway epithelial cells in controls and iPAH patients without any variations in fluorescence intensity (Supplemental Figure 1A). Coimmunostaining of CFTR and von Willebrand factor (VWF, an endothelial cell marker) confirmed the localization of CFTR in PAECs (Supplemental Figure 1B) and confirmed the reduction in CFTR expression in PAECs from iPAH patients (Supplemental Figure 1B).

As shown in Figure 2B, to examine CFTR at the ultrastructural level in PAECs and PASMCs, we analyzed the localization of CFTR using correlative electron microscopy (Figure 2B). As expected, in non-PAH PAs, CFTR was present in the luminal plasma membrane and in the cytosol of PAECs. Quantification of CFTR expression in PAECs and PASMCs via gold particle density measurement confirmed that CFTR expression was lower in PAs from iPAH patients than in those from non-PAH patients (Figure 2C). To better quantify the expression of CFTR in PAs from iPAH patients, we measured the mRNA levels of CFTR. We found that *CFTR* mRNA expression was strongly reduced (by 75%) in iPAH PAs compared with non-iPAH PAs (Figure 2D).

Given the prevalence of heterozygous *CFTR* mutations in the human population, we analyzed the presence of the most frequent *CFTR* mutations (Supplemental Table 1) in all iPAH patients in the study. No CFTR mutations were found in the iPAH patients, confirming that the changes in CFTR expression observed in these patients were independent of *CFTR* mutations.

Reduced CFTR expression and CFTR activation-mediated PA relaxation in MCT-exposed rats

Via quantitative PCR, we found that MCT exposure for 2 and 3 weeks progressively reduced *CFTR* mRNA expression in PAs during the development of PH by 65% and 75%, respectively (Figure 3A), while it did not alter *CFTR* mRNA expression in bronchi in the same animals (Figure 3B) or in

pulmonary veins (Supplemental Figure 2A). Assessment of the Fulton index confirmed the development of RV hypertrophy, indicating that PH induced by MCT exposure was present 2 weeks after exposure (Figure 3C). CFTR localization was examined via immunohistochemistry (Figure 3D) in PAECs in paraffin-embedded lung sections (red circles) and in PASMCs (red arrows) in lung sections from control and MCT-exposed rats (3 weeks post induction). We found reduced staining intensity in pulmonary vascular cells from rats with MCT-induced PH (Figure 3D). Immunofluorescence experiments on frozen lung sections confirmed that CFTR was localized in PAECs and PASMCs in lung sections from control and MCT-exposed rats. We did not detect any CFTR staining (Supplemental Figure 2B) in the PAs of MCT-exposed rats.

Next, we investigated the consequences of pharmacological modulation (activation or inhibition) of CFTR on PA contractility. As previously shown by Robert et al, CFTR activation induces PA relaxation in rats[8]. Using isolated PAs from control rats, we first assessed the consequence of pharmacological CFTR inhibition with the selective CFTR inhibitor[14] $CFTR_{inh172}$ (10 µmol/L) on the contractile response to different doses of KCl (ranging from 10 to 90 mmol/L). As shown in Figure 3E, the contractile response of PAs in response to increasing doses of KCl was unchanged in the presence of $CFTR_{inh172}$ (Figure 3E left panel, unchanged EC50 between DMSO- and $CFTR_{inh172}$-treated PAs). However, the amplitude of the contractile response to 60 mM KCl was significantly higher in PAs incubated with $CFTR_{inh172}$ than in PAs incubated with DMSO (Figure 3E right panel).

Using isolated PAs from MCT-treated rats (after 1, 2 and 3 weeks of MCT exposure), we found that the dose-response curve for KCl-induced contraction was progressively shifted to the left during the course of PH development (Supplemental Figure 3A). We also measured CFTR-dependent PA relaxation using increasing concentrations of the CFTR activator MPB91[8]. PA rings were preconstricted with 1 µM U46619 (a thromboxane A2 mimetic). Increasing concentrations of MPB91 produced progressive PA relaxation under control conditions (black curve) (Figure 3F). This response was progressively attenuated in PAs from MCT-exposed rats (Figure 3F): the relaxation produced by 300 µmol/L MPB91 was 32%, 60% and 80% lower than that produced by the control treatment after 1, 2 and 3 weeks of MCT exposure, respectively.

We next used a second CFTR activator, CFTRact-A1 (CactA1)[15]. Similar to MPB91, $C_{act}A1$ at increasing concentrations produced progressive PA relaxation under control conditions following preconstriction of PA rings with 1 µM U46619 (black curve) (Figure 4A). Importantly, this $C_{act}A1$-dependent relaxation was strongly reduced in the presence of 10 µmol/L or 30 µmol/L $CFTR_{inh172}$, suggesting that PA relaxation in response to $C_{act}A1$ was a consequence of CFTR activation. As shown in Figure 4B, $C_{act}A1$-induced relaxation was also strongly reduced in PAs from MCT-exposed rats (W3) (≈70% at 100 µmol/L $C_{act}A1$, Figure 4B). Next, we investigated the role of CFTR in PH induced by CH in rats (3 weeks at 10% O_2). $C_{act}A1$-dependent relaxation was strongly reduced (by more than 90% at 100 µmol/L $C_{act}A1$) in isolated PAs from CH-exposed rats compared to PAs from normoxia (Nx)-exposed rats (Figure 4C). MPB91-induced relaxation was 45% lower in isolated PAs from CH rats than in PAs from Nx-exposed rats (Supplemental Figure 3B). As demonstrated by the Fulton index, a strong increase in RV hypertrophy indicated that CH-exposed rats developed PH (Figure 4D). We found that *Cftr* mRNA expression was lower in PAs isolated from CH-exposed rats than in PAs isolated from Nx-exposed rats (Figure 4E); in addition, less CFTR staining was observed in PAs from CH-exposed rats (Figure 4F).

Moreover, the results showed that increasing concentrations of $C_{act}A1$ produced progressive relaxation of isolated PAs from healthy pigs (Supplemental Figure 3G).

Finally, increasing concentrations of VX770 (Ivacaftor), a CFTR potentiator approved to treat CF[16, 17], also produced progressive rat PA relaxation (black curve) (Supplemental Figure 3C). Importantly, this VX770-dependent PA relaxation was strongly reduced in PAs from MCT-exposed rats (W3) (by 70% at 200 µmol/L VX770, Supplemental Figure 3C).

Reduced CFTR activation-mediated relaxation in PAs from iPAH patients Confirming the vasoconstrictive effect on PAs in iPAH patients, we found that the dose-response curve of KCl-induced contraction was strongly shifted to the left for PAs from iPAH patients compared to PAs isolated from controls (Figure 5A); consistent with this finding, a smaller EC50 value was observed for PAs isolated from iPAH patients than for those isolated from control (Figure 5B).

Given the dose responses to CFTR activators previously obtained in rat and pig PAs (Figures 3 and 4), we challenged human control and iPAH-isolated PAs with 100 µmol/L MPB91, VX770 and CactA1

(Figure 5C-F). We found that all three activators produced significant relaxation in control arteries (MPB91, 38%; VX770, 28%; CactA1, 19%) (Figure 5F). (Figure 5C-E). Nevertheless, as shown in Figure 5F, relaxation was severely reduced in PAs from iPAH patients (MPB91, 6.15%; VX770, 5.18%; CactA1, 3%). The same volume of DMSO (vehicle) had a minimal impact on human PA relaxation (Figure 5F). These results demonstrate that CFTR is functionally expressed in human control PAs, where it contributes to the regulation of PA tone. The results also indicated that CFTR-mediated PA relaxation was strongly reduced in PAs from iPAH patients. As indicated in Supplemental Table 1, no *CFTR* mutations were found in iPAH patients.

Chronic in vivo inhibition of CFTR induced PH with exaggerated pulmonary vascular cell proliferation To evaluate whether loss of function of CFTR can contribute to initiation of PH, we chronically inhibited CFTR in healthy rats using $CFTR_{inh172}$ (2 mg/kg/d i.p.). After 2 weeks, $CFTR_{inh172}$-treated rats displayed significantly increased RV systolic pressure (RVSP) (Figure 6B), but the right ventricle was not hypertrophied (Fulton index, Figure 6A), and neither cardiac output (Figure 6C) nor systemic blood pressure (Figure 6D) was altered. In association with the increase in RVSP in $CFTR_{inh172}$-treated rats, we also measured a significant decrease in PA acceleration time (PAAT) by echocardiography (Supplemental Table 2). We did not measure any modifications in RV or left ventricular (LV) thickness, RV ejection time (RVET), cycle length (CL), heart rate (HR), PA velocity time integral (VTI Pa), or RV LV fractional shortening in $CFTR_{inh172}$-treated rats (Table 1).

To evaluate the consequence of CFTR inhibition on *in situ* pulmonary cell proliferation, we visualized proliferating lung cells by measuring the incorporation of 5-ethynyl-2'-deoxyuridine (EdU; pink nuclei and yellow arrow in Figure 6E) in $CFTR_{inh172}$-exposed rats. We detected very few EdU-positive cells in control lung parenchyma (DMSO-treated rats, Figure 6E left), whereas there were areas of intense pulmonary cell proliferation in $CFTR_{inh172}$-exposed rat lung parenchyma (Figure 6E right). The quantification results are shown in a bar graph in Figure 6F. $CFTR_{inh172}$-exposed rats exhibited increased numbers of lung proliferative cells, including PASMCs, as the numbers of α-smooth muscle actin (αSMA)- and EdU-positive cells were augmented (Figure 6F). As indicated in Figure 6G, greater accumulation of proliferating cells, as measured by immunostaining of Ki67 (a marker of cell proliferation), was observed in the media as well as in the endothelium in PAs from $CFTR_{inh172}$-

exposed rats compared to PAs from vehicle-exposed rats (Figure 6H-I). However, the percentages of Ki67-positive nuclei in adventitia and bronchi did not differ between $CFTR_{inh172}$-exposed rats and vehicle-exposed rats (Figure 6J).

Finally, Western blot analysis showed that P-AKT308, CD45 (a pan-leukocyte marker), serum albumin, VE-cadherin and transient receptor potential canonical channel 6 (TRPC6) levels were unchanged in the lungs of $CFTR_{inh172}$-exposed rats (Supplemental Figure 4). We also used Western blot analysis to evaluate the expression of CFTR protein in human PASMCs (hPASMCs) from control and iPAH patients. As illustrated in Figure 6K, CFTR protein (175 kDa, detected with an Alomone CFTR antibody) was present in control hPASMCs as well as hPASMCs cultured from iPAH patients. However, it was not present in three iPAH patients, and its levels were unchanged in one iPAH patient. The CFTR protein was strongly expressed in the positive control samples (human lung tissues) and absent in the negative control samples (A549 human adenocarcinomic alveolar basal epithelial cells), demonstrating the specificity of the CFTR bands. A549 cells are known to not express CFTR [18, 19]. The results indicated that the CFTR protein was weakly expressed in the majority of iPAH hPASMCs (Figure 6K). We obtained similar results using a second CFTR-specific antibody (175 kDa, CFTR antibody #596 from the CF Foundation) (Supplemental Figure 6). Therefore, we evaluated the role of CFTR only in hPASMC proliferation by pharmacologically inhibiting CFTR with 10 µmol/L $CFTR_{inh172}$ for 24 hours. This treatment enhanced the proliferation of control hPASMCs (Figure 6L). As shown in Supplemental Figure 7, we performed pathological assessment of the bronchial trees, livers and kidneys of $CFTR_{inh172}$-exposed rats. In $CFTR_{inh172}$-exposed rats, the large bronchi were patent and were delimited by normally structured walls that included collagen tissue, smooth muscle and cartilage rings. No bronchial inflammation could be detected in any specimen (Supplemental Figure 7i). In $CFTR_{inh172}$ rats, the liver architecture was maintained, with regular distribution of portal spaces and centrilobular veins. Neither portal fibrosis nor inflammation was identified in any of the samples. Hepatocytes were distributed along thin trabeculae. No centrilobular inflammation was observed (Supplemental Figure 7ii). Finally, the structure of the renal cortex was maintained in all specimens, and glomeruli were well represented within the cortex without hyaline involution. Glomerular inflammation, interstitial fibrosis and inflammation were absent. Renal tubules were lined

by regular cuboidal/cylindrical epithelial cells, and tubule dilation was not observed. The renal medullae did not appear to be altered. Renal vessels were patent without parietal thickening. No thrombi were visible (Supplemental Figure 7 iii and iv).

CFTR dysfunction or inhibition was associated with PA remodeling

Lung distal vessel muscularization was assessed by immunostaining (αSMA = smooth muscle marker, VWF = endothelial cell marker) (Figure 7A). $CFTR_{inh172}$-treated rats displayed a significantly increased percentages of small vessel muscularization (Figure 7A and Supplemental Figure 5A). We also found that the percentages of nonmuscularized vessels (VWF-positive vessels) were significantly lower in the lungs of *F508delCftr*-mutated rats than in those of wild-type (WT) rats, while the percentages of muscularized vessels (αSMA- and VWF-positive vessels) were significantly higher in *F508delCftr*-mutated rats than in WT rats (Figure 7B, Supplemental Figure 5B). We further analyzed PA thickening in lung samples from 10 CF patients (Supplemental Material). We observed PA wall, bronchial artery, intimal and medial thickening without obstructive thrombotic lesions, while we did not observe any plexiform lesions or pulmonary vein remodeling. As expected, PAs from non-CF and non-PAH patients did not show any morphological alterations (Figure 7C). However, CF patients displayed substantial arterial remodeling in comparison with controls (Figure 7D), as determined by the total wall (media+intima) thickness (Figure 7C) (21.7%±0.7 *vs* 12.4%±0.4). Echocardiography revealed that 2 CF patients had PH with severe RV dysfunction, while 4 CF patients had moderate PH (not shown). The extent of PA wall thickening in CF patients was mild in comparison with the same parameter in iPAH patients (40%; data not shown). Importantly, CF patients have variable percent predicted forced expiratory volume in 1 second ($ppFEV_1$) values, which could influence PA remodeling. As presented in Figure 7E, we did not find any correlation between the wall thickness percentage and $ppFEV_1$, suggesting that the PA remodeling observed in CF patients was partly independent of hypoxia/lung parenchymal destruction.

Chronic in vivo inhibition of CFTR induced exaggerated PH in MCT-exposed rats

As shown in Figure 6, rats with chronic CFTR inhibition displayed modest but significant increases in RVSP. Therefore, we exposed rats with chronic CFTR inhibition and vehicle-exposed rats to MCT (60 mg/kg). One week before MCT exposure, the animals were treated daily with vehicle or $CFTR_{inh172}$ (2

mg/kg/d i.p.). Then, the animals were exposed to MCT (60 mg/kg) or saline and continuously exposed to vehicle or $CFTR_{inh172}$ for two weeks (Figure 8A). *In vivo* CFTR inhibition increased the severity of MCT-induced PH, as demonstrated by elevated RVSP values in CFTR-inhibited rats (Figure 8B) with no modification of RV hypertrophy, total peripheral resistance (TPR) or mean carotid artery pressure (Figure 8C-E). We also found that RV end diastolic pressure (RV EDP) was higher in MCT- and $CFTR_{inh172}$-treated animals than in MCT- and DMSO-treated animals (Figure 8F). Finally, we found that the RV contractility index was lower in MCT- and $CFTR_{inh172}$-treated animals than in MCT- and DMSO-treated animals (Figure 8G). These results demonstrate that CFTR dysfunction predisposes rats to PH development under MCT exposure.

DISCUSSION

Using a combination of histology, myograph recording, molecular biology, and *ex vivo* and *in vivo* approaches, we obtained several major findings. First, CFTR is functionally expressed in the PAs of humans, rats and pigs, contributing to PA tone. Second, CFTR expression and CFTR-mediated PA relaxation are severely reduced in iPAH and decrease progressively during the development of experimental PH. Third, long-term inhibition of CFTR significantly increases RVSP and distal neomuscularization and exacerbates pulmonary vascular cell proliferation. Fourth, lungs from patients with severe CF and recently implemented *F508delcftr* rat models are characterized by PA remodeling.

Pulmonary vascular disease, particularly PH, is not well characterized in CF. PH has been estimated via right heart catheterization to occur in 26-63% of patients with CF[20]. Similarly, in one study, RV catheterization demonstrated that among individuals in the Florida CF cohort who underwent lung transplantation, 63.2% of CF patients had PH[21]. In another CF cohort (78 adults with CF), PA enlargement (an indicator of PH) was associated with increases in pulmonary vascular hemodynamics (mPAP, pulmonary capillary wedge pressure (PCWP), PVR) in severe CF and with decreased survival[11]. The occurrence of PH in CF patients could reflect other factors, such as lung hyperinflammation, lung destruction or pulmonary vascular matrix alterations[11]; it is not necessarily only directly related to CFTR dysfunction in PAs. Here, we found that the PA wall thickness in CF patients (*F508delCFTR*) was not correlated with $ppFEV_1$, suggesting that the PA remodeling observed in CF patients was partly independent of hypoxia/lung parenchymal destruction and was due mostly to *CFTR* mutation. Indeed, we demonstrated that *F508delCftr* rats developed pulmonary vessel neomuscularization without an abnormal lung phenotype, and CFTR-dependent Cl^- secretion is impaired in the nasal airways of *F508delcftr* mutant rats[22]. This feature is remarkable, as the concomitant study on the lungs of these animals did not show any CF-related alterations, such as inflammation or bronchial accumulation. We also excluded heterozygous *CFTR* mutations in our iPAH cohort by genotyping the *CFTR* gene in all patients included in the study. These results suggest that CFTR dysfunction could predispose patients to or facilitate pulmonary vascular remodeling independently of lung parenchymal destruction.

Exposure to CH has been found to downregulate CFTR in human lung epithelial cells[23]. The main molecule activated by hypoxia exposure is hypoxia inducible factor-1 alpha (HIF-1α), which regulates the expression of CFTR[24]. Chromatin immunoprecipitation has revealed a binding site for HIF-1α in the *CFTR* gene[24]. Consequently, HIF-1α overexpression leads to altered short circuit measurements and changes in transepithelial fluid movement[24]. Overexpression of HIF-1α is a hallmark of PAH and experimental PH that contributes to PA remodeling[25]. Here, we found that CFTR expression was severely downregulated in PAs from patients with iPAH and an experimental rat model of PH, suggesting that these decreases in CFTR expression could partly be due to overexpression of HIF-1α. In contrast with the present results, *Cftr* deficiency in mice has been found to diminish hypoxic vasoconstriction, and *cftr*$^{-/-}$ mice are protected against hypoxic PH[26]. Such discrepancy among humans, rats and mice has also been observed for the role of the K^+ channel KCNK3 in the development of PAH. There is strong evidence that *KCNK3* deficiency contributes to the development of PH in humans[27] and rats[28]. *kcnk3*$^{-/-}$ mice are protected from PH induced by CH exposure[29], indicating that the mouse model does not fully recapitulate the pathogenesis of PH in humans, particularly concerning the role of ion channels.

Robert et al. previously demonstrated that CFTR activation mediates relaxation of PA and aorta relaxation in a dose-dependent manner[8]. CFTR activation-mediated relaxation (of PAs or the aorta) is independent of the endothelium[8, 30]. Aorta relaxation induced by vasoactive intestinal peptide (VIP) or other cAMP agonists is reduced in aortas from *cftr*$^{-/-}$ mice, indicating that CFTR could be physiologically activated by cAMP agonists in these vessels[30]. Indeed, in epithelial cells, physiological activation of CFTR requires phosphorylation of the regulatory R domain by protein kinase A[31] and ATP hydrolysis by the nucleotide-binding domains[32]. In aortas from CFTR-F508del pigs, CFTR mutation decreases aortic responsiveness by affecting smooth muscle Ca^{2+} handling[33]. In human airways, TRPC6 is an essential component of the receptor-activated Ca^{2+} influx machinery in both smooth muscle and epithelial cells, linking Ca^{2+} signaling to CFTR pathobiology[34]

In mice, *cftr* deficiency is associated with increased contraction of the aorta, suggesting that loss or dysfunction of CFTR alters the physiological regulation of vascular tone. In the present study, we found that CFTR was downregulated in iPAH patients as well as in two experimental models of PH. This downregulation was correlated with a severe reduction in CFTR-dependent PA relaxation in a model associated with a predisposition to PA vasoconstriction. To explain the role played by CFTR in the regulation of PA tone, we postulate that channel activation is associated with relaxation[8, 30]. Alternatively, CFTR may regulate PA tone independently of its role as a Cl^- channel *via* other mechanisms, including modification of lipid trafficking and Ca^{2+} handling in smooth muscle cells[26, 33, 35]. In addition to its channel function, the CFTR protein can interact with and regulate a considerable number of proteins because it has a PDZ binding domain in its C-terminal domain[36]. Studies have shown that CFTR can interact with NHERF1 (an EB^+/H^+ regulatory factor), ezrin-radixin-moesin-binding phosphoprotein 50 (EBP50) and CFTR accessory protein 70 (CAP 70)[37]. CFTR can also interact with and regulate other ion channels, such as epithelial sodium channel (ENaC)[38], TRPC6[26, 34], and renal outer medullary potassium channel 2 (ROMK2)[39].

In the present study, we found that *in vivo* CFTR inhibition accelerated the development of PH after MCT exposure in association with increased RV EDP and reduced RV contractility, indicating that CFTR inhibition facilitates RV dysfunction in the context of MCT exposure. Several experimental and clinical studies have reported the occurrence of myocardial dysfunction in CF patients, which affects systolic and diastolic heart function[40]. CF patients may have poorer cardiac and peripheral hemodynamic function than healthy subjects[41]. Pallin et al demonstrated that in CF, severity of genotype is associated with cardiac impairment[42]. Via echocardiography, we did not detect alterations in RV or LV function in rats with CFTR inhibition. In a zebrafish model, CFTR inhibition with $CFTR_{inh172}$ has been found to alter the development of the heart in the blastula stage. Moreover, loss of CFTR impairs cardiac development, resulting in atrial dilation, pericardial edema, and decreased HR[43]. In $cftr^{-/-}$ mice, the lack of CFTR leads to increased myocardial contractility at baseline, which may trigger problematic myocardial remodeling in CF patients independent of lung diseases[44].

In MCF-7 breast cancer cells, CFTR controls cellular quiescence. Indeed, CFTR inhibition downregulates the Wnt and AURKA signaling pathways and upregulates the p53 signaling pathway, leading to an increase in cell proliferation[45]. In intestinal cells, knockdown of CFTR enhances cell proliferation *via* inhibition of the hedgehog pathway[46]. In addition, CFTR activation suppresses glioblastoma cell proliferation[47]. Consistent with the cell proliferative phenotype, CF is associated with an elevated predisposition to cancer[48] and is not restricted to the digestive tract[49]. Many studies have reported that CFTR is downregulated in several cancer types and that CFTR dysfunction promotes the development of cancer *in vitro* and *in vivo*, suggesting that CFTR acts as a tumor suppressor protein[48]. Moreover, CFTR inhibition with $CFTR_{inh172}$ increases endothelial permeability in human PAECs by reducing VE-cadherin and p120 catenin membrane expression[9]. Here, we found that CFTR inhibition ($CFTR_{inh172}$) enhanced the proliferation rate of control hPASMCs, suggesting that reduced expression of CFTR in PAH PAs also favors PA remodeling. We also found that CFTR protein expression in hPASMCs from individuals with iPAH remained at high levels in some iPAH patients, suggesting that a pharmacological strategy activating CFTR might be of interest for patients with PAH who retain residual levels of CFTR expression, possibly within the frame of personalized therapy.

In conclusion, we provide evidence that the CFTR channel contributes to PA tone in humans, pigs and rats; that PA CFTR expression is reduced in iPAH and in 2 different experimental models of PAH; and that CFTR inhibition increases vascular cell proliferation. Altogether, these alterations may contribute to the development of PH.

SOURCES OF FUNDING

F.A. receives funding from the National Funding Agency for Research: ANR-18-CE14-0023. F.A. also receives funding from the Fondation du Souffle et Fonds de Dotation Recherche en Santé Respiratoire, from the Fondation Lefoulon-Delalande and from the Fondation Legs Poix. F.P. is supported by the Legs Poix, Chancellerie des Universités de Paris. M.L. is supported by the Therapeutic Innovation Doctoral School (ED569).

CONFLICT OF INTEREST/DISCLOSURES

M.H. has relationships with drug companies, including Actelion, Bayer, GSK, Novartis, and Pfizer. In addition to being an investigator in trials involving these companies, M.H. has other relationships with consultancy services and is a member of scientific advisory boards. The other authors have no conflicts of interest.

REFERENCES

1. Simonneau G, Montani D, Celermajer DS, Denton CP, Gatzoulis MA, Krowka M, Williams PG, Souza R. Haemodynamic definitions and updated clinical classification of pulmonary hypertension. *Eur Respir J* [Internet] 2019 [cited 2019 Apr 18]; 53Available from: https://www.ncbi.nlm.nih.gov/pmc/articles/PMC6351336/.

2. Humbert M, Guignabert C, Bonnet S, Dorfmüller P, Klinger JR, Nicolls MR, Olschewski AJ, Pullamsetti SS, Schermuly RT, Stenmark KR, Rabinovitch M. Pathology and pathobiology of pulmonary hypertension: state of the art and research perspectives. *Eur Respir J* [Internet] 2019 [cited 2019 Apr 18]; 53Available from: https://www.ncbi.nlm.nih.gov/pmc/articles/PMC6351340/.

3. Vonk Noordegraaf A, Chin KM, Haddad F, Hassoun PM, Hemnes AR, Hopkins SR, Kawut SM, Langleben D, Lumens J, Naeije R. Pathophysiology of the right ventricle and of the pulmonary circulation in pulmonary hypertension: an update. *Eur. Respir. J.* 2019; 53.

4. Lambert M, Capuano V, Olschewski A, Sabourin J, Nagaraj C, Girerd B, Weatherald J, Humbert M, Antigny F. Ion Channels in Pulmonary Hypertension: A Therapeutic Interest? *Int J Mol Sci* 2018; 19.

5. Papp R, Nagaraj C, Zabini D, Nagy BM, Lengyel M, Skofic Maurer D, Sharma N, Egemnazarov B, Kovacs G, Kwapiszewska G, Marsh LM, Hrzenjak A, Höfler G, Didiasova M, Wygrecka M, Sievers LK, Szucs P, Enyedi P, Ghanim B, Klepetko W, Olschewski H, Olschewski A. Targeting TMEM16A to reverse vasoconstriction and remodelling in idiopathic pulmonary arterial hypertension. *Eur. Respir. J.* 2019; 53.

6. Riordan JR, Rommens JM, Kerem B, Alon N, Rozmahel R, Grzelczak Z, Zielenski J, Lok S, Plavsic N, Chou JL. Identification of the cystic fibrosis gene: cloning and characterization of complementary DNA. *Science* 1989; 245: 1066–1073.

7. McCuaig S, Martin JG. How the airway smooth muscle in cystic fibrosis reacts in proinflammatory conditions: implications for airway hyper-responsiveness and asthma in cystic fibrosis. *Lancet Respir Med* 2013; 1: 137–147.

8. Robert R, Savineau J-P, Norez C, Becq F, Guibert C. Expression and function of cystic fibrosis transmembrane conductance regulator in rat intrapulmonary arteries. *European Respiratory Journal* 2007; 30: 857–864.

9. Totani L, Plebani R, Piccoli A, Di Silvestre S, Lanuti P, Recchiuti A, Cianci E, Dell'Elba G, Sacchetti S, Patruno S, Guarnieri S, Mariggiò MA, Mari VC, Anile M, Venuta F, Del Porto P, Moretti P, Prioletta M, Mucilli F, Marchisio M, Pandolfi A, Evangelista V, Romano M. Mechanisms of endothelial cell dysfunction in cystic fibrosis. *Biochimica et Biophysica Acta (BBA) - Molecular Basis of Disease* 2017; 1863: 3243–3253.

10. Fraser KL, Tullis DE, Sasson Z, Hyland RH, Thornley KS, Hanly PJ. Pulmonary hypertension and cardiac function in adult cystic fibrosis: role of hypoxemia. *Chest* 1999; 115: 1321–1328.

11. Wells JM, Farris RF, Gosdin TA, Dransfield MT, Wood ME, Bell SC, Rowe SM. Pulmonary artery enlargement and cystic fibrosis pulmonary exacerbations: a cohort study. *The Lancet Respiratory Medicine* 2016; 4: 636–645.

12. Selimovic N, Bergh C-H, Andersson B, Sakiniene E, Carlsten H, Rundqvist B. Growth factors and interleukin-6 across the lung circulation in pulmonary hypertension. *Eur. Respir. J.* 2009; 34: 662–668.

13. Ratjen F. Pulmonary artery hypertension: an underrated disease manifestation in cystic fibrosis? *Lancet Respir Med* 2016; 4: 596–598.

14. Ma T, Thiagarajah JR, Yang H, Sonawane ND, Folli C, Galietta LJV, Verkman AS. Thiazolidinone CFTR inhibitor identified by high-throughput screening blocks cholera toxin–induced intestinal fluid secretion [Internet]. American Society for Clinical Investigation; 2002 [cited 2020 Mar 9].Available from: https://www.jci.org/articles/view/16112/pdf.

15. Namkung et al. - 2013 - Novel Amino-Carbonitrile-Pyrazole Identified in a .pdf [Internet]. [cited 2019 Jul 15].Available from: https://www-ncbi-nlm-nih-gov.gate2.inist.fr/pmc/articles/PMC3876813/pdf/mol.113.086348.pdf.

16. Ramsey BW, Bell SC, Wainwright CE, Sermet-Gaudelus I, Yen K. A CFTR Potentiator in Patients with Cystic Fibrosis and the G551D Mutation. *n engl j med* 2011; : 10.

17. Van Goor F, Hadida S, Grootenhuis PDJ, Burton B, Cao D, Neuberger T, Turnbull A, Singh A, Joubran J, Hazlewood A, Zhou J, McCartney J, Arumugam V, Decker C, Yang J, Young C, Olson ER, Wine JJ, Frizzell RA, Ashlock M, Negulescu P. Rescue of CF airway epithelial cell function in vitro by a CFTR potentiator, VX-770. *Proc. Natl. Acad. Sci. U.S.A.* 2009; 106: 18825–18830.

18. Hamai H, Keyserman F, Quittell LM, Worgall TS. Defective CFTR increases synthesis and mass of sphingolipids that modulate membrane composition and lipid signaling. *J Lipid Res* 2009; 50: 1101–1108.

19. Ren H, Birch NP, Suresh V. An Optimised Human Cell Culture Model for Alveolar Epithelial Transport. *PLoS One* [Internet] 2016 [cited 2021 Mar 15]; 11Available from: https://www.ncbi.nlm.nih.gov/pmc/articles/PMC5079558/.

20. Hayes D, Tobias JD, Mansour HM, Kirkby S, McCoy KS, Daniels CJ, Whitson BA. Pulmonary hypertension in cystic fibrosis with advanced lung disease. *Am. J. Respir. Crit. Care Med.* 2014; 190: 898–905.

21. Tonelli AR, Fernandez-Bussy S, Lodhi S, Akindipe OA, Carrie RD, Hamilton K, Mubarak K, Baz MA. Prevalence of pulmonary hypertension in end-stage cystic fibrosis and correlation with survival. *J. Heart Lung Transplant.* 2010; 29: 865–872.

22. Dreano E, Bacchetta M, Simonin J, Galmiche L, Usal C, Slimani L, Sadoine J, Tesson L, Anegon I, Concordet J-P, Hatton A, Vignaud L, Tondelier D, Sermet-Gaudelus I, Chanson M, Cottart C-H. Characterization of two rat models of cystic fibrosis-KO and F508del CFTR-Generated by Crispr-Cas9. *Animal Model Exp Med* 2019; 2: 297–311.

23. Bartoszewska S, Kamysz W, Jakiela B, Sanak M, Króliczewski J, Bebok Z, Bartoszewski R, Collawn JF. miR-200b downregulates CFTR during hypoxia in human lung epithelial cells. *Cellular & Molecular Biology Letters* [Internet] 2017 [cited 2019 Jul 15]; 22Available from: https://cmbl.biomedcentral.com/articles/10.1186/s11658-017-0054-0.

24. Zheng W, Kuhlicke J, Jäckel K, Eltzschig HK, Singh A, Sjöblom M, Riederer B, Weinhold C, Seidler U, Colgan SP, Karhausen J. Hypoxia inducible factor-1 (HIF-1)-mediated repression of cystic

fibrosis transmembrane conductance regulator (CFTR) in the intestinal epithelium. *FASEB J.* 2009; 23: 204–213.

25. Shimoda LA, Yun X, Sikka G. Revisiting the role of hypoxia-inducible factors in pulmonary hypertension. *Current Opinion in Physiology* 2019; 7: 33–40.

26. Tabeling C, Yu H, Wang L, Ranke H, Goldenberg NM, Zabini D, Noe E, Krauszman A, Gutbier B, Yin J, Schaefer M, Arenz C, Hocke AC, Suttorp N, Proia RL, Witzenrath M, Kuebler WM. CFTR and sphingolipids mediate hypoxic pulmonary vasoconstriction. *Proc Natl Acad Sci U S A* 2015; 112: E1614–E1623.

27. H LR, V C, B G, M H, D M, F A. Implication of Potassium Channels in the Pathophysiology of Pulmonary Arterial Hypertension [Internet]. Biomolecules Biomolecules; 2020 [cited 2020 Sep 10].Available from: https://pubmed.ncbi.nlm.nih.gov/32882918/.

28. Lambert M, Capuano V, Boet A, Tesson L, Bertero T, Nakhleh MK, Remy S, Anegon I, Pechoux C, Hautefort A, Rucker-Martin C, Manoury B, Domergue V, Mercier O, Girerd B, Montani D, Perros F, Humbert M, Antigny F. Characterization of Kcnk3-Mutated Rat, a Novel Model of Pulmonary Hypertension. *Circ. Res.* 2019; 125: 678–695.

29. Kitagawa MG, Reynolds JO, Wehrens XHT, Bryan RM, Pandit LM. Hemodynamic and Pathologic Characterization of the TASK-1−/− Mouse Does Not Demonstrate Pulmonary Hypertension. *Front Med (Lausanne)* [Internet] 2017 [cited 2020 Mar 3]; 4Available from: https://www.ncbi.nlm.nih.gov/pmc/articles/PMC5660113/.

30. Robert R, Norez C, Becq F. Disruption of CFTR chloride channel alters mechanical properties and cAMP-dependent Cl^- transport of mouse aortic smooth muscle cells: CFTR chloride channels in smooth muscle. *The Journal of Physiology* 2005; 568: 483–495.

31. Becq F, Merten MD, Voelckel MA, Gola M, Figarella C. Characterization of cAMP dependent CFTR-chloride channels in human tracheal gland cells. *FEBS Lett.* 1993; 321: 73–78.

32. Hanrahan JW. Revisiting Cystic Fibrosis Transmembrane Conductance Regulator Structure and Function. *Proceedings of the American Thoracic Society* 2004; 1: 17–21.

33. Guo JJ, Stoltz DA, Zhu V, Volk KA, Segar JL, McCray PB, Roghair RD. Genotype-specific alterations in vascular smooth muscle cell function in cystic fibrosis piglets. *Journal of Cystic Fibrosis* 2014; 13: 251–259.

34. Antigny F, Norez C, Dannhoffer L, Bertrand J, Raveau D, Corbi P, Jayle C, Becq F, Vandebrouck C. Transient receptor potential canonical channel 6 links Ca2+ mishandling to cystic fibrosis transmembrane conductance regulator channel dysfunction in cystic fibrosis. *Am. J. Respir. Cell Mol. Biol.* 2011; 44: 83–90.

35. Michoud M-C, Robert R, Hassan M, Moynihan B, Haston C, Govindaraju V, Ferraro P, Hanrahan JW, Martin JG. Role of the cystic fibrosis transmembrane conductance channel in human airway smooth muscle. *Am. J. Respir. Cell Mol. Biol.* 2009; 40: 217–222.

36. Boucherot A, Schreiber R, Kunzelmann K. Role of CFTR's PDZ1-binding domain, NBF1 and Cl− conductance in inhibition of epithelial Na+ channels in Xenopus oocytes. *Biochimica et Biophysica Acta (BBA) - Biomembranes* 2001; 1515: 64–71.

37. Wang X, Venable J, LaPointe P, Hutt DM, Koulov AV, Coppinger J, Gurkan C, Kellner W, Matteson J, Plutner H, Riordan JR, Kelly JW, Yates JR, Balch WE. Hsp90 cochaperone Aha1 downregulation rescues misfolding of CFTR in cystic fibrosis. *Cell* 2006; 127: 803–815.

38. Stutts MJ, Canessa CM, Olsen JC, Hamrick M, Cohn JA, Rossier BC, Boucher RC. CFTR as a cAMP-dependent regulator of sodium channels. *Science* 1995; 269: 847–850.

39. McNicholas CM, Nason MW, Guggino WB, Schwiebert EM, Hebert SC, Giebisch G, Egan ME. A functional CFTR-NBF1 is required for ROMK2-CFTR interaction. *Am. J. Physiol.* 1997; 273: F843-848.

40. Labombarda F, Saloux E, Brouard J, Bergot E, Milliez P. Heart involvement in cystic fibrosis: A specific cystic fibrosis-related myocardial changes? *Respir Med* 2016; 118: 31–38.

41. Bisch AL, Wheatley CM, Baker SE, Peitzman ER, Van Iterson EH, Laguna TA, Morgan WJ, Snyder EM. Cystic Fibrosis Transmembrane Conductance Regulator Genotype, Not Circulating Catecholamines, Influences Cardiovascular Function in Patients with Cystic Fibrosis. *Clin Med Insights Circ Respir Pulm Med* 2019; 13: 1179548419835788.

42. Pallin M, Keating D, Kaye DM, Kotsimbos T, Wilson JW. Subclinical Left Ventricular Dysfunction is Influenced by Genotype Severity in Patients with Cystic Fibrosis. *Clin Med Insights Circ Respir Pulm Med* 2018; 12: 1179548418794154.

43. Liu Y, Lin Z, Liu M, Liao H, Chen Y, Zhang X, Chan HC, Zhou B, Rao L, Sun H. CFTR deficiency causes cardiac dysplasia during zebrafish embryogenesis and is associated with dilated cardiomyopathy. *Mech. Dev.* 2020; : 103627.

44. Jiang K, Jiao S, Vitko M, Darrah R, Flask CA, Hodges CA, Yu X. The impact of Cystic Fibrosis Transmembrane Regulator Disruption on cardiac function and stress response. *J. Cyst. Fibros.* 2016; 15: 34–42.

45. Li A-Q, Sun Z-P, Liu X, Yang J-S, Jin F, Zhu L, Jia W-H, De Vos S, Van Stappen G, Bossier P, Yang W-J. The chloride channel cystic fibrosis transmembrane conductance regulator (CFTR) controls cellular quiescence by hyperpolarizing the cell membrane during diapause in the crustacean Artemia. *J. Biol. Chem.* 2019; 294: 6598–6611.

46. Liu K, Jin H, Guo Y, Liu Y, Wan Y, Zhao P, Zhou Z, Wang J, Wang M, Zou C, Wu W, Cheng Z, Dai Y. CFTR interacts with Hsp90 and regulates the phosphorylation of AKT and ERK1/2 in colorectal cancer cells. *FEBS Open Bio* 2019; 9: 1119–1127.

47. Zhong X, Chen H-Q, Yang X-L, Wang Q, Chen W, Li C. CFTR activation suppresses glioblastoma cell proliferation, migration and invasion. *Biochem. Biophys. Res. Commun.* 2019; 508: 1279–1285.

48. Amaral MD, Quaresma MC, Pankonien I. What Role Does CFTR Play in Development, Differentiation, Regeneration and Cancer? *Int J Mol Sci* 2020; 21.

49. Maisonneuve P, Marshall BC, Knapp EA, Lowenfels AB. Cancer Risk in Cystic Fibrosis: A 20-Year Nationwide Study From the United States. *JNCI: Journal of the National Cancer Institute* 2013; 105: 122–129.

FIGURE LEGENDS

Figure 1: Expression of CFTR protein in PAECs and PASMCs in control and iPAH patients. **C**FTR immunostaining in paraffin-embedded lung sections from control and iPAH patients. PAEC and PASMC staining is visible (blue arrow in control patients and red arrow in iPAH patients). i) CFTR staining in concentric lesions. ii and iii) CFTR staining in plexiform lesions. iv) CFTR staining in remodeled PAs from PH patients with COPD. Scale, 100 μm.

Figure 2: CFTR expression is reduced in iPAH patients. (A) Localization of CFTR by correlative light and electron microscopy in PAs from non-PAH and iPAH patient lungs after CFTR labeling. PAECs and PASMCs exhibited gold particles (white arrows) in the cytosol and small amounts at the plasma membrane. (B-C) Quantification of CFTR expression in PAECs (upper panel) and PASMCs (lower panel) from non-PAH and iPAH patients via gold particle density measurement in PAECs and PASMCs (3 control and 3 iPAH). Scale, 1 μm or 200 nm. EC, endothelial cell; Col, collagen; E, elastic lamina; N, nucleus; PAH, pulmonary arterial hypertension; and PASMC, pulmonary arterial smooth muscle cell. (D) mRNA expression levels of CFTR in PAs isolated from non-PAH patients and patients with iPAH (n=8 for both non-PAH patients and patients with iPAH). *$p< 0.05$ *vs. control.* The experimental data were analyzed using the Mann-Whitney test.

Figure 3: CFTR expression and relaxation of PAs evoked by CFTR activation are reduced in MCT-exposed rats. (A) mRNA expression levels of CFTR in PAs isolated from controls and MCT-exposed rats (at week 1, week 2 and week 3) (n=6-8 rats). (B) mRNA expression levels of CFTR in bronchi isolated from controls and MCT-exposed rats (at week 1, week 2 and week 3) (n=6-8 rats). (C) Fulton indexes (right ventricle weight/left ventricle weight + septum (S) weight) of the animals used for quantitative PCR (6-8 rats). (D) CFTR immunostaining in paraffin-embedded lung sections from control and MCT-PH rats. PAEC and PASMC staining is visible (red arrows). Scale, 50 μm. (E) Dose-response curve (normalized to K100) established by applying increasing concentrations of KCl to isolated PAs from control rats in the presence of DMSO or $CFTR_{inh172}$ (10 μM). Right, corresponding quantification of the EC50 and contractile amplitude at 90 mM KCl (n=5-6 rats). (F) Relaxant response to increasing concentrations of the CFTR activator MPB91 (MPB91; 1 μmol/L to 300

µmol/L) in PA segments from controls and MCT-exposed rats (at week 1, week 2 and week 3) precontracted with U46619 (1 µM). Right, corresponding graph showing the percent relaxation in response to MPB91 at 300 µmol/L (n=5-8 rats). ns: nonsignificant. *$p< 0.05$ **$p<0.01$ *vs. control.* The data were analyzed using one-way ANOVA followed by Tukey's *post hoc* test.

Figure 4: CFTR activation by $C_{act}A1$ induces concentration-dependent relaxation of rat and pig PAs. (A) Relaxant response to increasing concentrations of the CFTR activator $C_{act}A1$ (1 µmol/L to 200 µmol/L) in rat PA segments precontracted with U46619 (1 µM) in the presence of vehicle (DMSO) or $CFTR_{inh172}$ used at 10 µmol/L or 30 µmol/L. (B) Left panel, relaxant response to increasing concentrations of C_{act}-A1 ($C_{act}A1$, 1 µmol/L to 200 µmol/L) in control and MCT-exposed rats (3 weeks). Right panel, corresponding graph showing the percent relaxation in response to $C_{act}A1$ at 100 µmol/L. (C) Left panel relaxant response to increasing concentrations of $C_{act}A1$ ($C_{act}A1$, 1 µmol/L to 200 µmol/L) in PA segments isolated from rats exposed to Nx or CH (3 weeks). Right panel, corresponding graph showing the percent relaxation in response to 100 µmol/L $C_{act}A1$. (D) Corresponding plot showing the Fulton index. (E) mRNA expression levels of *Cftr* in PAs isolated from controls and CH-exposed rats (at week 3) (n=4-5 rats). (F) CFTR immunostaining in paraffin-embedded lung sections from control and MCT-PH rats: PAEC and PASMC staining is visible. Scale, 50 µm. ns: nonsignificant. *$p< 0.05$ **$p<0.01$ *vs. control.* The data were analyzed using the Mann-Whitney test.

Figure 5: CFTR is functionally expressed in human control PAs. (A) Concentration-response curve (normalized to K100) established by applying increasing concentrations of K^+ to PA rings isolated from human control patients and patients with iPAH. (B) EC50 quantification. In human control and iPAH PA rings precontracted with U46619 (1 µM), the CFTR activator MPB91 (100 µmol/L) (C), the CFTR activator $C_{act}A1$ (100 µmol/L) (D) and the CFTR potentiator VX770 (100 µmol/L) (E) separately produced PA relaxation. (F) Corresponding graph showing the percent relaxation in response to these CFTR activators 10 min after CFTR activation (n=7 controls *vs* 6 iPAH samples).

Figure 6: In vivo inhibition of CFTR-induced early hemodynamic signs of PH and exaggerated proliferation of pulmonary vascular cells. (A) Quantification of the Fulton index (right ventricle weight/left ventricle weight + septum (S) weight) (B). Quantification of RVSP (mmHg). (C)

Quantification of cardiac output (CO, mL/min). (D) Quantification of mean carotid pressure (mCP, mmHg) (n=8-9 rats). (E) Immunofluorescence staining and confocal imaging of frozen rat lung sections labeled with Click-iT EdU (pink nuclei=EdU-positive nuclei=proliferating cells (yellow arrow)) in combination with α-SMA (green) and DAPI (blue). (F) Upper panel, quantification of the percentages of proliferating lung cells (n=7 rats). Lower panel, quantification of the percentages of αSMA+ EdU-positive cells (n=7 rats). (G) Immunostaining against Ki67 (proliferation marker) in paraffin-embedded rat lung sections from DMSO- and $CFTR_{inh172}$-exposed rats. (H) Quantification of the percentages of Ki67-positive nuclei in the media in PAs (n=5). (I) Quantification of the percentages of Ki67-positive nuclei in the endothelium in PAs (n=5). (J) Quantification of the percentages of Ki67-positive nuclei in the bronchi (n=5). (K) Representative Western blots of CFTR in hPASMCs from controls (n=4) and iPAH patients (n=4), in human lungs (positive control) and in human adenocarcinomic alveolar basal epithelial cells (A549 cells) (negative control). (L) Percentages of proliferating cells among $CFTR_{inh172}$ (10 μM)-treated hPASMCs compared with DMSO-treated hPASMCs (n=7 patients). ns: nonsignificant. *$*p<0.05$, **$*p<0.01$ vs*. $CFTR_{inh172}$ *or DMSO*. The experimental data were analyzed using the Mann-Whitney test.

Figure 7: CFTR dysfunction or inhibition promotes PA remodeling. (A) Immunofluorescence labeling and confocal imaging of lungs from DMSO- and $CFTR_{inh172}$-treated rats stained for α-SMA (green) and VWF (red). Right panel, percentage of muscularized vessels (100 vessels per rat, n=7 rats) as measured by immunostaining against αSMA and VWF. (B) Immunofluorescence labeling and confocal imaging of lungs from WT and homozygous F508delCftr rats stained for α-SMA (green) and vWF (red). Right panel, percentage of muscularized vessels (100 vessels per rat, n=7 rats) as measured by immunostaining against αSMA and VWF. (C) PAs from CF patients showing a thickening of the wall in connection with hypertrophy of smooth muscle cells (i) as well as irregular remodeling of the wall (ii). CF patients also presented with thickened bronchial arteries with increased thickness of the intima and the media (iii) without obstructive thrombotic lesions. Non-CF and non-PH pulmonary arteries without morphological alterations are also shown (iv). (D) Quantification of the PA wall thickness (media+intima) (9 non-CF and control patients (control), 10 CF patients). (E) Correlation

between $ppFEV_1$ value and PA wall thickness (media+intima). ****p< 0.001 vs. control*. The experiments were analyzed using the Mann-Whitney test.

Figure 8: In vivo chronic inhibition of CFTR predisposes rats to develop PH under MCT exposure. (A) Experimental protocol used. (B) Quantification of the Fulton index (right ventricle weight/left ventricle weight + septum (S) weight). (C) Quantification of RVSP (mmHg). (D) Quantification of cardiac output (CO, mL/min). (E) Quantification of PVR (evaluated by the RVSP/CO ratio) (n=8-9 rats). (F) Quantification of RV EDP (mmHg). (G) Quantification of the RV contractility index (1/s) (n=8-9 rats).

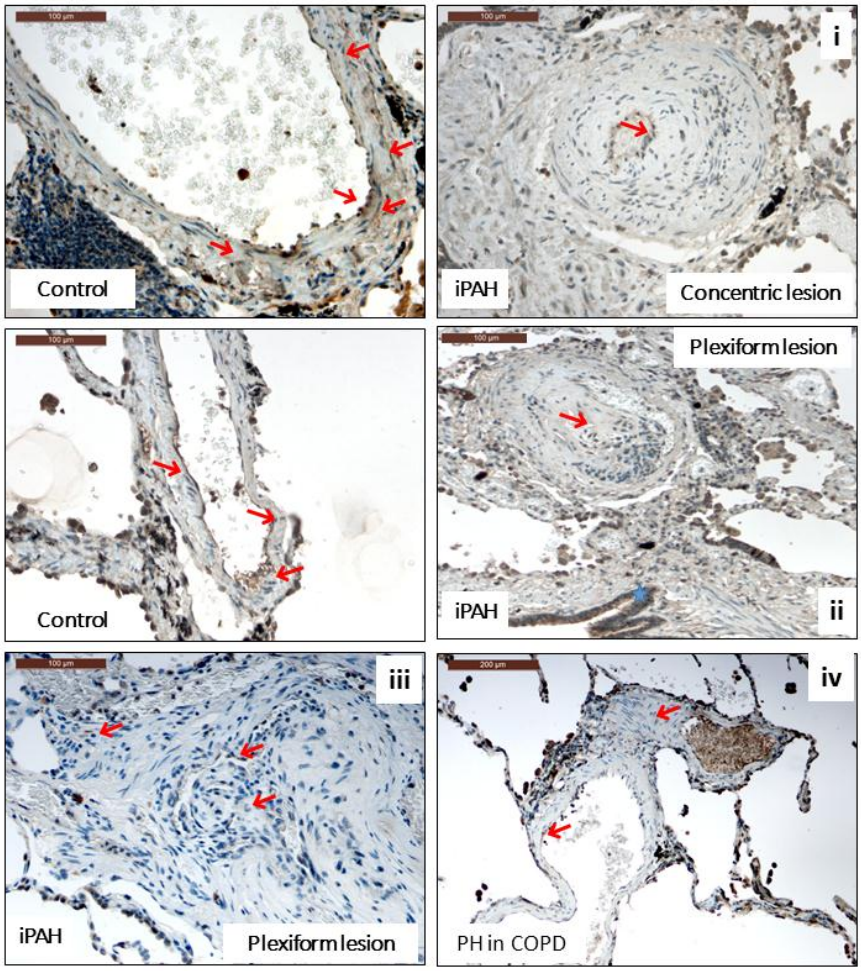
Control
i
iPAH
Concentric lesion
Control
Plexiform lesion
iPAH
ii
iii
iPAH
Plexiform lesion
iv
PH in COPD

Figure 1

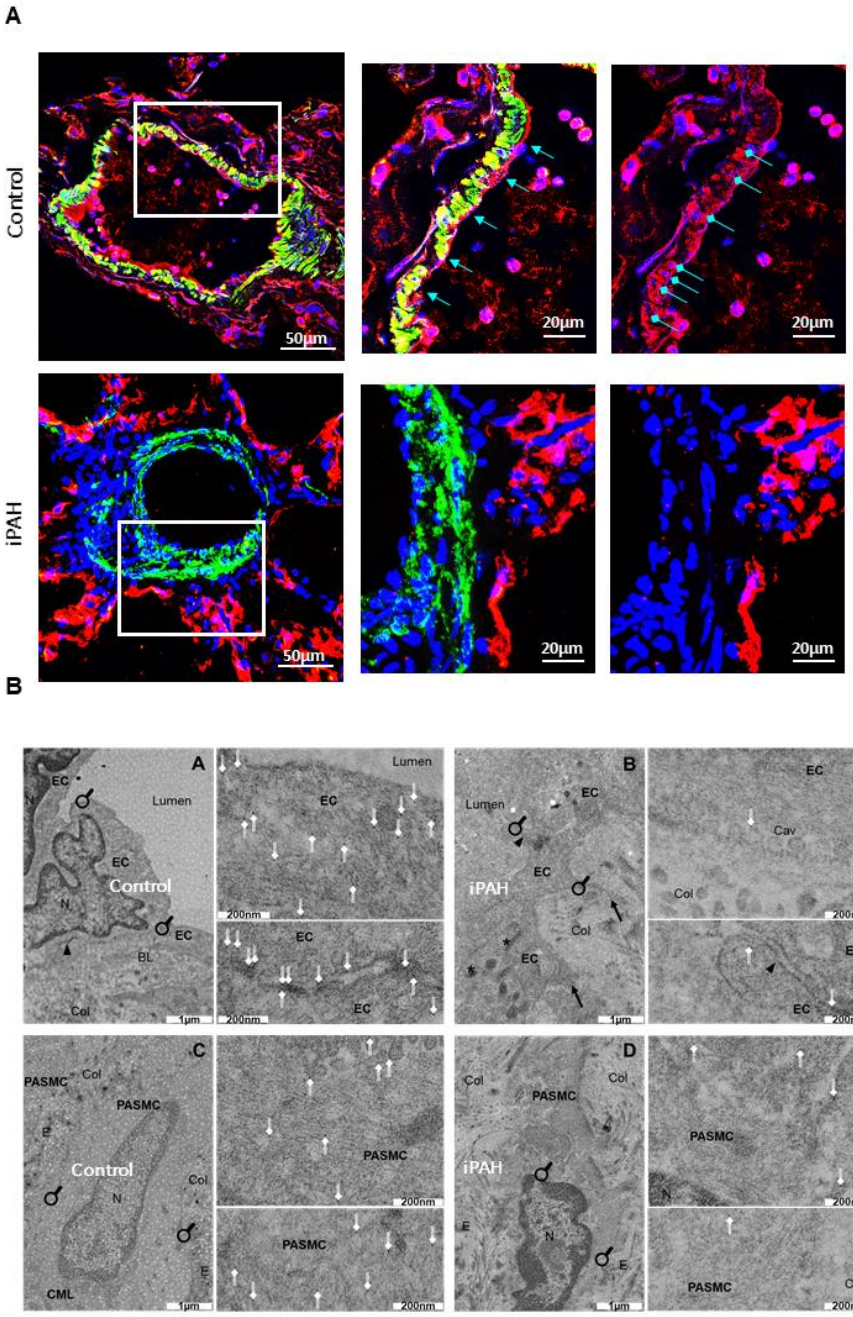
A
Control
iPAH
50µm
20µm
B
Lumen
EC
Control
iPAH
Cav
Col
BL
PASMC
CML
1µm
200nm
C
PASMC
PAEC
Gold particules number / µm²
Gold particules number / 10 µm²
Control
iPAH
D
Pulmonary arteries
CFTR mRNA relative expression

Figure 2

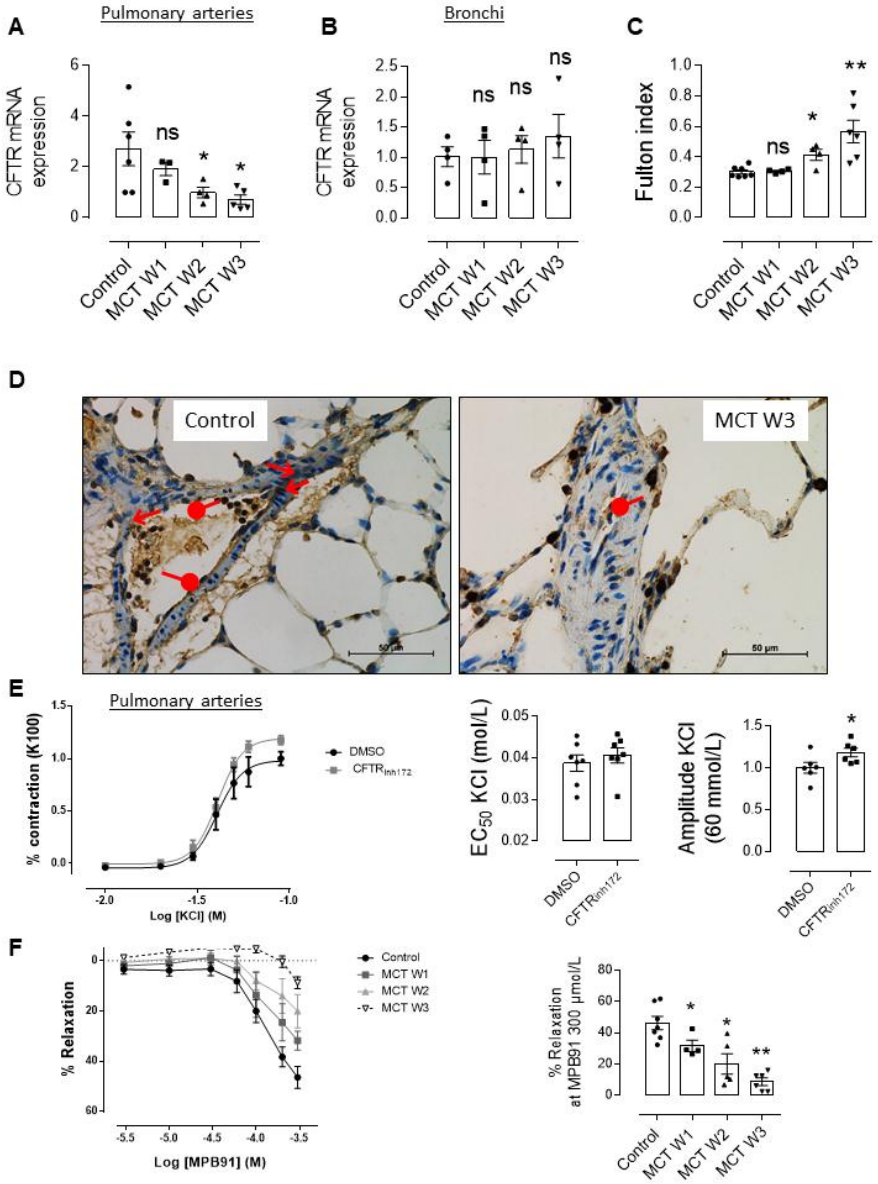
A
Pulmonary arteries
CFTR mRNA expression
ns
*
*
Control
MCT W1
MCT W2
MCT W3
B
Bronchi
CFTR mRNA expression
ns
ns
ns
C
Fulton index
ns
*
**
D
Control
MCT W3
50 µm
E
Pulmonary arteries
% contraction (K100)
Log [KCl] (M)
DMSO
CFTRinh172
EC50 KCl (mol/L)
Amplitude KCl (60 mmol/L)
F
% Relaxation
Log [MPB91] (M)
Control
MCT W1
MCT W2
MCT W3
% Relaxation at MPB91 300 µmol/L

Figure 3

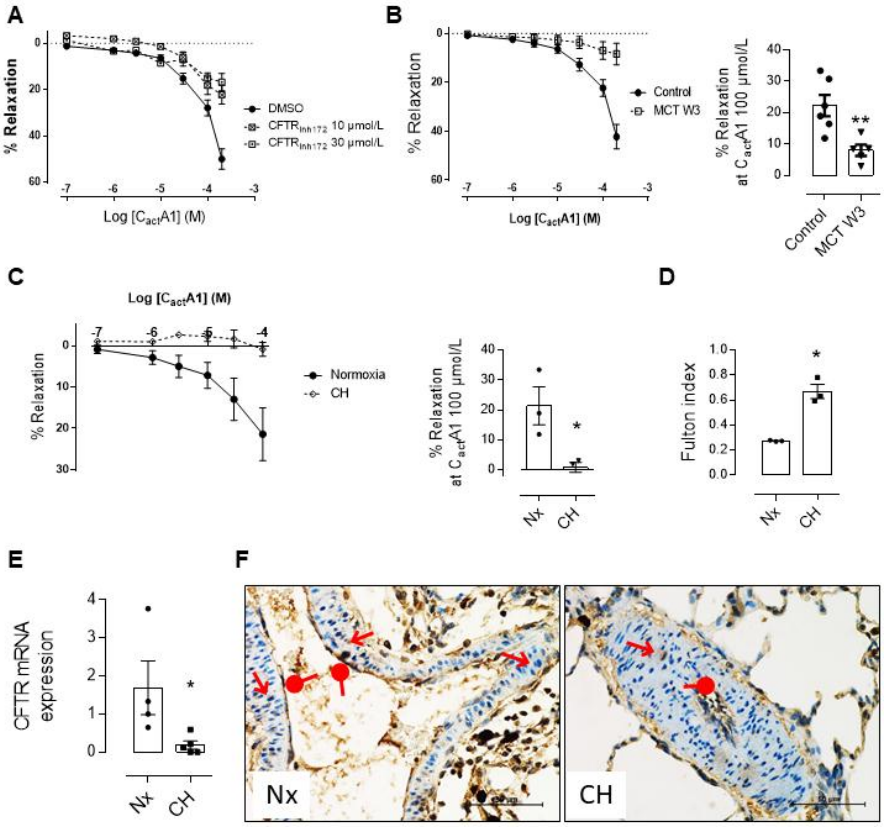
A
% Relaxation
DMSO
CFTRinh172 10 µmol/L
CFTRinh172 30 µmol/L
Log [CactA1] (M)
B
% Relaxation
Control
MCT W3
Log [CactA1] (M)
% Relaxation at CactA1 100 µmol/L
Control
MCT W3
C
Log [CactA1] (M)
% Relaxation
Normoxia
CH
% Relaxation at CactA1 100 µmol/L
Nx
CH
D
Fulton index
Nx
CH
E
CFTR mRNA expression
Nx
CH
F
Nx
CH

Figure 4

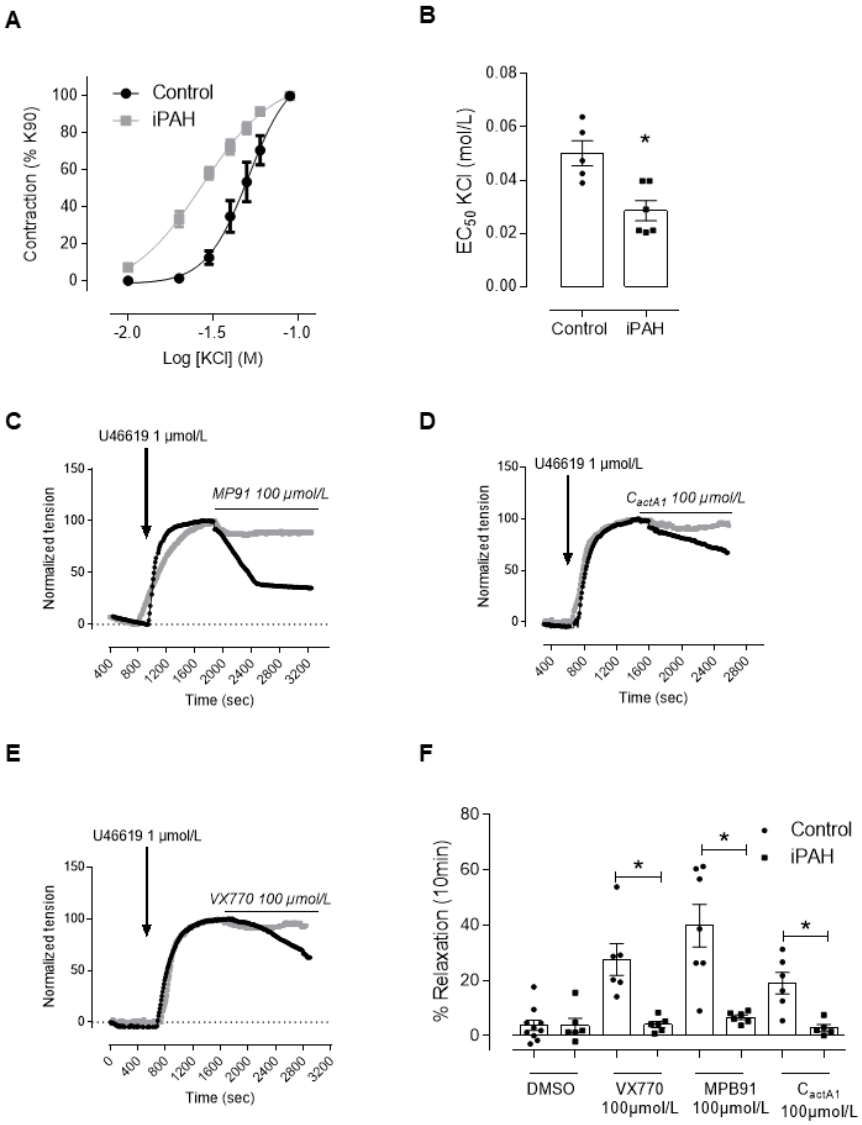
A
Control
iPAH
Contraction (% K90)
Log [KCl] (M)
B
EC50 KCl (mol/L)
Control
iPAH
C
U46619 1 µmol/L
MP91 100 µmol/L
Normalized tension
Time (sec)
D
U46619 1 µmol/L
CactA1 100 µmol/L
Normalized tension
Time (sec)
E
U46619 1 µmol/L
VX770 100 µmol/L
Normalized tension
Time (sec)
F
% Relaxation (10min)
Control
iPAH
DMSO
VX770 100µmol/L
MPB91 100µmol/L
CactA1 100µmol/L

Figure 5

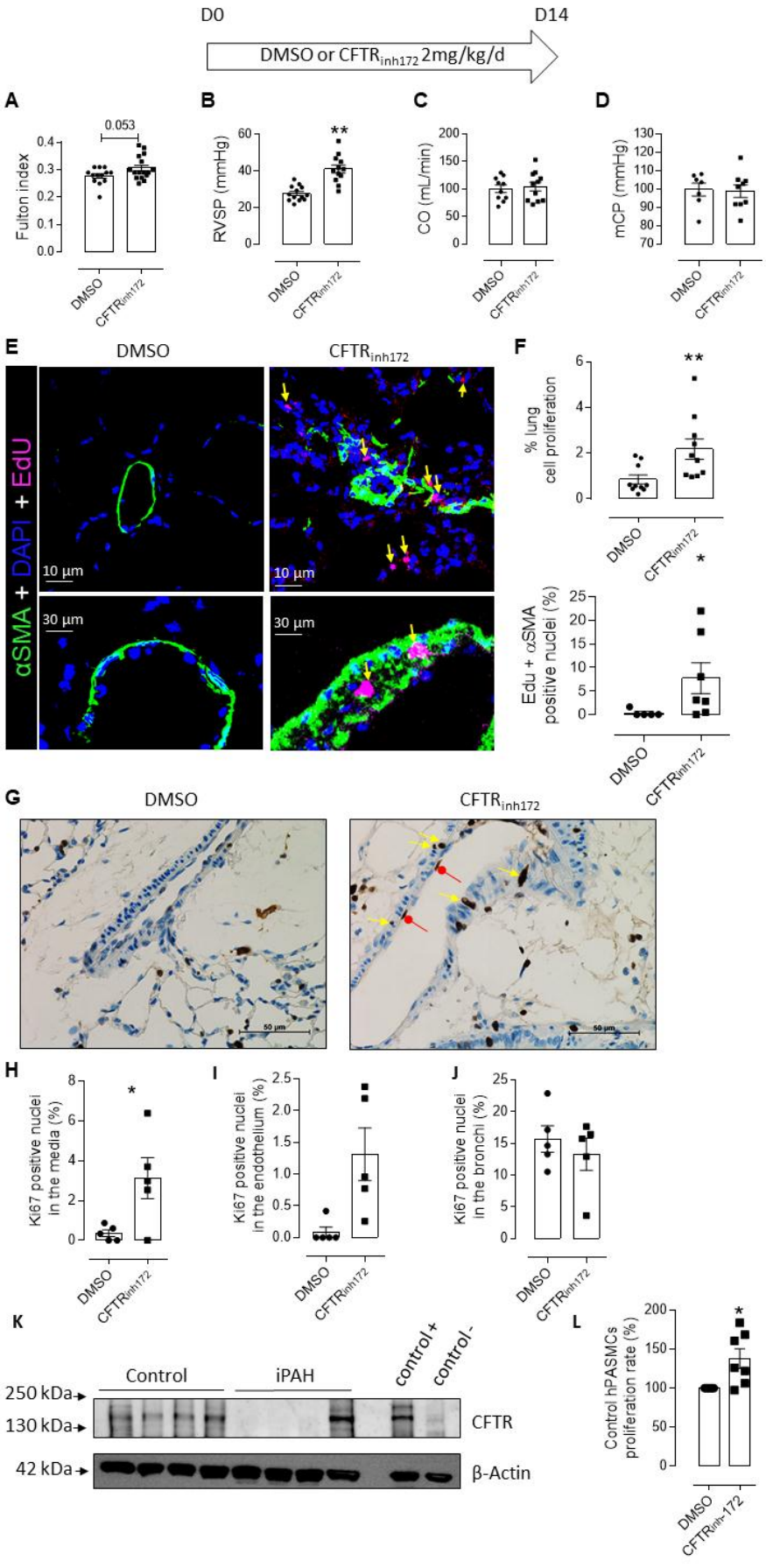
D0
D14
DMSO or CFTRinh172 2mg/kg/d
A
B
C
D
Fulton index
RVSP (mmHg)
CO (mL/min)
mCP (mmHg)
0.053
**
DMSO
CFTRinh172
E
DMSO
CFTRinh172
αSMA + DAPI + EdU
10 µm
30 µm
F
% lung cell proliferation
Edu + αSMA positive nuclei (%)
*
G
DMSO
CFTRinh172
50 µm
H
Ki67 positive nuclei in the media (%)
I
Ki67 positive nuclei in the endothelium (%)
J
Ki67 positive nuclei in the bronchi (%)
K
Control
iPAH
control+
control-
250 kDa
130 kDa
42 kDa
CFTR
β-Actin
L
Control hPASMCs proliferation rate (%)
CFTRinh-172

Figure 6

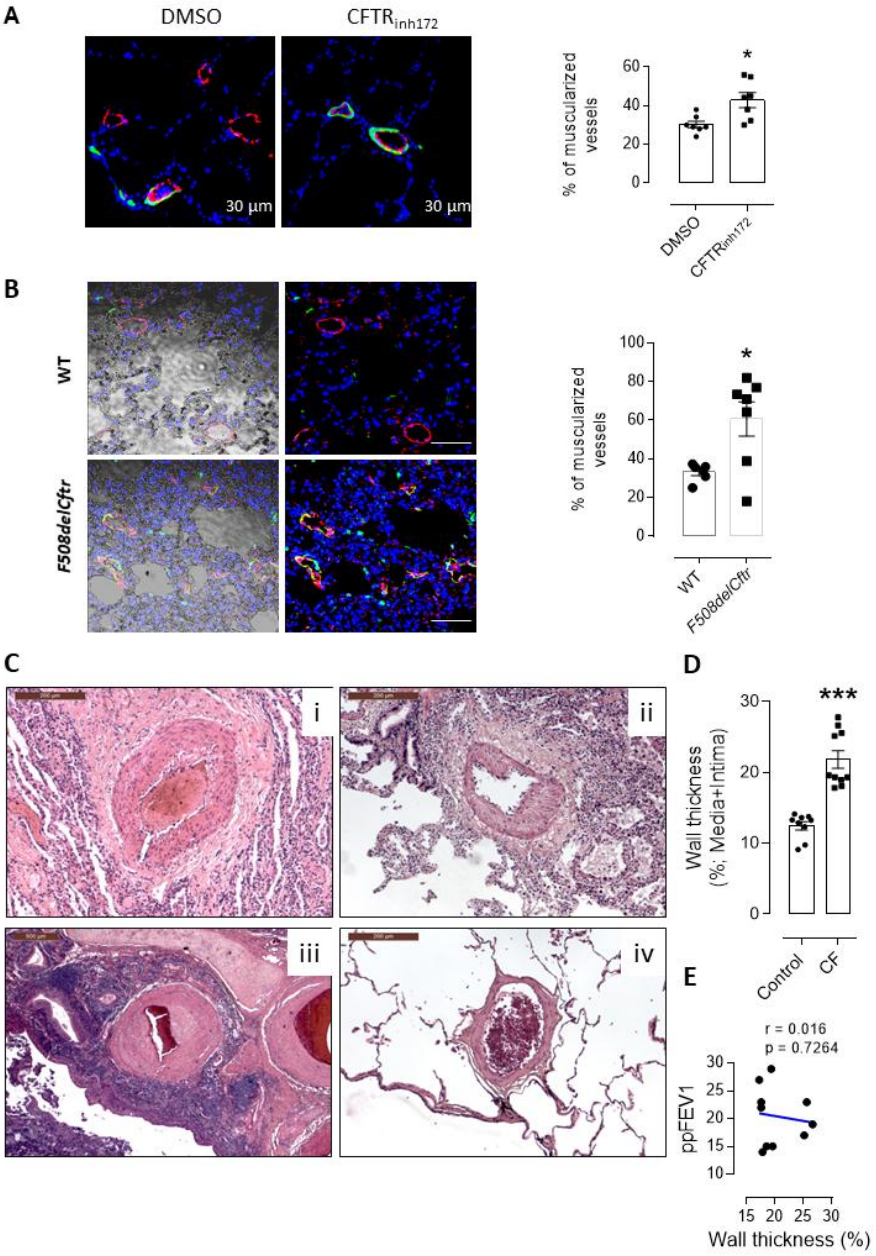
A
DMSO
CFTR$_{inh172}$
30 µm
30 µm
% of muscularized vessels
60
40
20
0
*
DMSO
CFTR$_{inh172}$
B
WT
F508delCftr
% of muscularized vessels
100
80
60
40
20
0
*
WT
F508delCftr
C
i
ii
iii
iv
D
Wall thickness (%; Media+Intima)
30
20
10
0
***
Control
CF
E
r = 0.016
p = 0.7264
ppFEV1
30
25
20
15
10
15 20 25 30
Wall thickness (%)

Figure 7

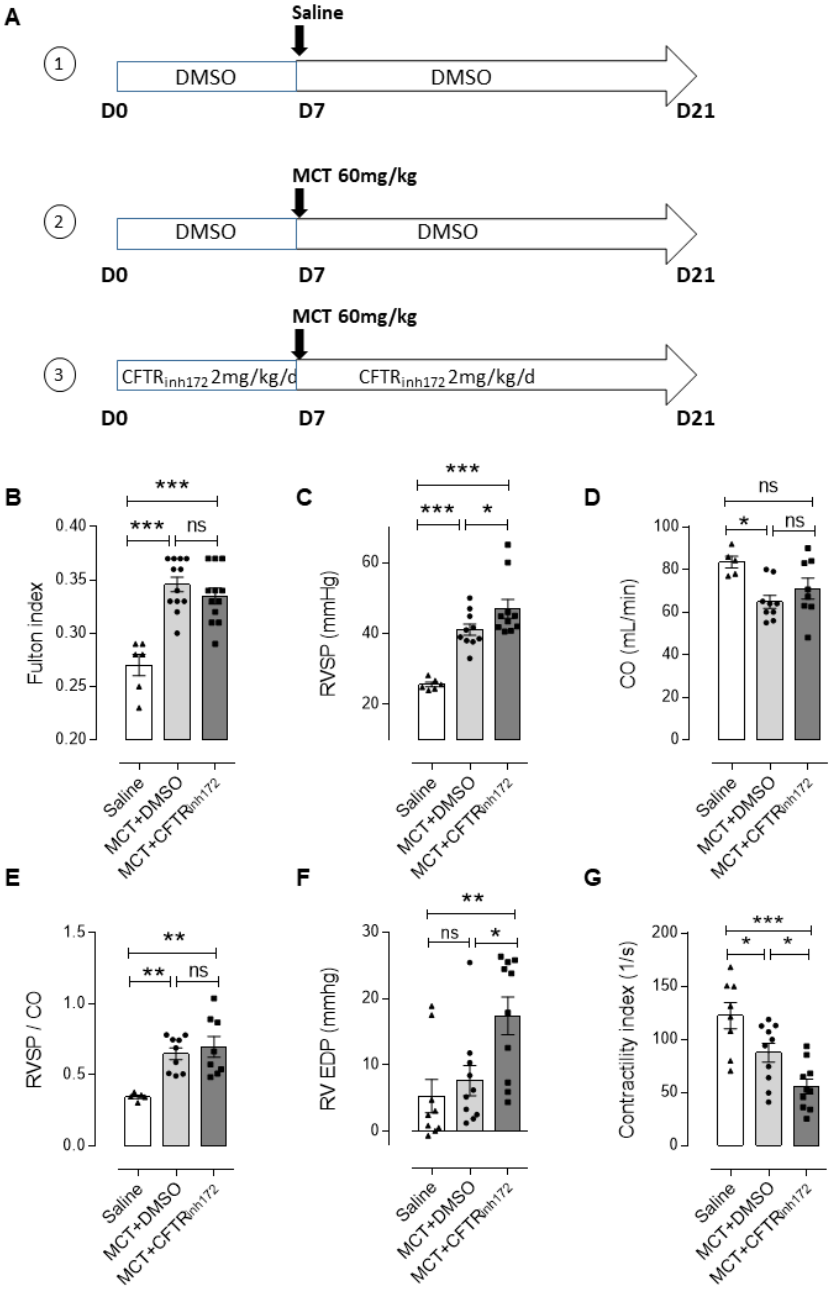
A
Saline
1
DMSO
DMSO
D0
D7
D21
MCT 60mg/kg
2
DMSO
DMSO
D0
D7
D21
MCT 60mg/kg
3
CFTRinh172 2mg/kg/d
CFTRinh172 2mg/kg/d
D0
D7
D21
B
Fulton index
C
RVSP (mmHg)
D
CO (mL/min)
E
RVSP / CO
F
RV EDP (mmhg)
G
Contractility index (1/s)
Saline
MCT+DMSO
MCT+CFTRinh172
ns
*
**
***

Figure 8

Supplemental Material

Involvement of CFTR in the pathogenesis of pulmonary arterial hypertension

Hélène Le Ribeuz[1,2,3], Lucie To[1,2,3], Maria-Rosa Ghigna[1,2,3], Clémence Martin[4,5], Chandran Nagaraj[6], Elise Dreano[7] Catherine Rucker-Martin[1,2,3], Barbara Girerd[1,2,3], Jérôme Bouliguan[8], Christine Pechoux[9], Mélanie Lambert[1,2,3], Angèle Boet[1,2,3], Justin Issard[1,2,3], Olaf Mercier[1,2,3], Konrad Hoetzenecker[10], Boris Manoury[11], Frédéric Becq[12], Pierre-Régis Burgel[4, 5], Charles-Henry Cottart[7], Andrea Olschewski[5,13] Isabelle Sermet-Gaudelus[7], Frédéric Perros[1,2,3], Marc Humbert[1,2,3], David Montani[1,2,3] and Fabrice Antigny[1,2,3]

Affiliations

[1]*Université Paris-Saclay, Faculté de Médecine, Le Kremlin-Bicêtre, France (H. L.-R., L. T., M.-R. G., C. R.-M., B. G., J. B., M. L., A. B., O. M., F. P., D. M., M. H., F. A.)*

[2]*INSERM UMR_S 999 « Hypertension pulmonaire: Physiopathologie et Innovation Thérapeutique », Hôpital Marie Lannelongue, Le Plessis-Robinson, France (H. L.-R., L. T., M.-R. G., C. R.-M., B. G., M. L., A. B., O. M., F. P., D. M., M. H., F. A.)*

[3]*Assistance Publique – Hôpitaux de Paris (AP-HP), Service de Pneumologie et Soins Intensifs Respiratoires, Centre de Référence de l'Hypertension Pulmonaire, Hôpital Bicêtre, Le Kremlin-Bicêtre, France. (H. L.-R., L. T., M.-R. G., C. R.-M., B. G., M. L., A. B., O. M., F. P., D. M., M. H., F. A.)*

[4] *Assistance Publique – Hôpitaux de Paris (AP-HP), Dept of Respiratory Medicine, Centre de Référence Maladie Rare Mucoviscidose, ERN-Lung, Cochin Hospital, 27 rue du Faubourg Saint Jacques, 75014 Paris, France (C. M., P.-R. B.)*

[5] *Inserm U1016, Institut Cochin, Université de Paris, Paris, France (C. M., P.-R. B.)*

[6] *Ludwig Boltzmann Institute for Lung Vascular Research, Graz, Austria (C. N., A. O.)*

[7] *Inserm U1151 – CNRS UMR 8253 – Institut Necker Enfants Malades, Centre Maladie Rare Mucoviscidose, ERN Lung, Université de Paris, Paris, France (E. D., C.-H. C., I. S.-G.)*

[8] *Laboratoire de Génétique Moléculaire, Pharmacogénétique et Hormonologie, Assistance Publique-Hôpitaux de Paris (AP-HP), Hôpital Bicêtre, Le Kremlin-Bicêtre, France; INSERM UMR-1185, Université Paris Saclay, Faculté de Médecine, Le Kremlin Bicêtre, France (J. B).*

[9] *GABI, INRA, AgroParisTech, Université Paris-Saclay, 78350 Jouy-en-Josas, France (C. P.)*

[10] *Department of Thoracic Surgery, Medical University of Vienna, Vienna, Austria (K.H.)*

[11] *Signalisation et Physiopathologie Cardiovasculaire – UMR_S 1180, Univ. Paris-Sud, INSERM, Université Paris-Saclay, Châtenay-Malabry, France (B. M.)*

[12] *Laboratoire Signalisation et Transports Ioniques Membranaires, Université de Poitiers, 86073 Poitiers Cedex 9, France (F. B.)*

[13] *Experimental Anesthesiology, Department of Anesthesiology and Intensive Care Medicine, Medical University of Graz, Graz, Austria (A. O.).*

Corresponding author: Fabrice Antigny, INSERM UMR_S 999, Hôpital Marie Lannelongue, 133, Avenue de la Résistance, F-92350 Le Plessis Robinson, France. Fax: (33) 1 40 94 25 22, Tel.: (33) 1 40 94 22 99, e-mail: fabrice.antigny@universite-paris-sacaly.fr

Online Methods

Material and methods

Chemicals- Monocrotaline (MCT), and Sildenafil were obtained from Sigma. U46619 were obtained from R&D Systems. CFTRAct-A1 ($C_{act}A1$) was obtained from Calbiochem $CFTR_{inh172}$ was obtained from Tebu-Bio. MPB-91 was synthesized as previously described (20).

Animals- The animal facility is licensed by the French Ministry of Agriculture (agreement N° C92-019-01). This study was approved by the Committee on the Ethics of Animal Experiments (CEEA26 CAP Sud). The animal experiments were performed conforming to the guidelines from Directive 2010/63/EU on 22 September 2010 of the European Parliament on the protection of animals used for scientific purposes and complied with the French institution's guidelines for animal care and handling. Male Wistar rats (4 weeks old) were used in four experimental protocols:

1. PH was induced by a single MCT injection (60 mg/kg, s.c.). MCT was dissolved in 1 N HCl and neutralized with 1 N NaOH. Control animals received the same volume of saline solution.

2. For chronic hypoxia (CH) model, Wistars rats were placed 3 weeks in hypoxia (10 % O2) in normobaric condition. Normaxia Wistar rats were placed in the same room during 3 weeks.

3. 5. Daily exposure (2 mg/kg, i.p.) during one month to the selective CFTR blocker $CFTR_{inh172}$. $CFTR_{inh172}$ compound was dissolved in DMSO. Control animals received the same volume of DMSO.

Patients- Human lung specimens were obtained at the time of lung transplantation in 7 patients with PAH and at the time of lobectomy or pneumonectomy for localized lung cancer from 10 control subjects. PAH patients underwent genetic counseling and signed written informed consent for genetic analysis. No mutation was identified in 7 patients. These 7 patients were included in the GWAS analysis of Ma and collaborators[1], and were not carriers of *KCNK3*, BMPR2 or other mutation. These patients correspond to idiopathic PAH (iPAH). In the lung specimens from control subjects, pulmonary arteries were studied at distance from tumor areas. Transthoracic echocardiography was performed preoperatively in the control subjects to rule out PH. Patients studied were part of the French Network on Pulmonary Hypertension, a program approved by our institutional Ethics Committee, and had given written informed consent (Protocol N8CO-08- 003, ID RCB: 2008-A00485-50, approved on June 18, 2008).

Human lung tissue samples were obtained from patients with idiopathic pulmonary arterial hypertension (IPAH) who underwent lung transplantation at the Department of Surgery, Division of Thoracic Surgery, Medical University of Vienna, Vienna, Austria. The protocol and tissue usage were approved by the institutional ethics committee (976/2010) and written patient consent was obtained before lung transplantation. The patient characteristics included: age at the time of the transplantation, weight, height, sex, mean pulmonary arterial pressure (mPAP) measured by right heart catheterization, pulmonary function tests, as well as the medical therapy. The chest computed tomography (CT) scans and right heart catheterization (RHC) data were reviewed by experienced pathologists and pneumologists to verify the diagnoses. Healthy donor lung tissue was obtained from the same source.

Human PASMC and PAEC culture- Human lung specimens were obtained at the time of a lobectomy or pneumonectomy for localized lung cancer from control subjects. Pulmonary arteries were studied at a distance from tumor areas. Human PAECs and PASMCs were cultured as previously described [2] and were used for the study between passages 3 and 5. PASMC or PAEC were isolated from pulmonary arteries obtained during lobectomy or pneumonectomy of localized lung cancer from control subjects. Pulmonary arteries were excised at distance from tumor areas. Patients studied were

part of a program approved by our institutional Ethics Committee, and had given written informed consent (ID RCB: 2018-A01252-53, approved on June 18, 2006)

CF patients-Human lung tissues containing non-cartilaginous airways were obtained at lung transplantation from 10 nonsmoking CF adults. Seven patients were homozygous for the *Phe508del-CFTR* mutation and the other three were Phe508del/minimal function (G542X, Q890X or N1303K). Pre-lung-transplant-percent predicted forced expiratory volume in 1 second ($ppFEV_1$ ranged from 14 % to 29%, and all patients were under long-term oxygen therapy for chronic hypoxemia. All patients were chronically infected with P. aeruginosa. Lung tissue samples obtained at transplantation were fixed in 10% neutral buffered formalin by inflation-immersion and embedded in paraffin. To reduce the potential sampling bias related to irregular distribution of morphological abnormalities in CF patients, tissues were chosen randomly among two to four blocks (depending on tissue availability) from each patient. The study obtained agreement of the local ethics committee (CPP Ile de France II; number 1072) for the use of samples of human origin.

F508del-Cftr rats were generated using CRISPR-Cas9 technology and genome editing techniques for the introduction into the genome of single-stranded oligo donor sequences by microinjection into rat zygotes, as described[3]. The target sites were based on exon 12; donor DNA generated a codon deletion at F508. *F508delCftr* heterozygous rats were inbred to generate F508del homozygous rats and WT littermates. Laxative (PEG 3350 – KleanPrep®) was added to the drinking water. To reduce mortality, *F508delCftr* rats were fed with a liquid diet composed of DietGel 31M and Boost (Clear H2O®, Ssniff-Spezialdiäten GmbH; Soest, Germany) as their respective WT littermates. Then, chow mixed with laxative-containing water (DietGel + laxative) was progressively introduced in the diet. Both male (n= 5) and female (n= 9) rats were used for histological study. All animal care performed in the Paris facility were approved by the Animal Experimentation Ethics Committee of Paris Descartes University.

Control pig-We used seven Landrace SHAM male piglets for other surgery protocols to minimize the number of scarified animal. Sham pigs just had left thoracotomy. Pulmonary artery from SHAM animal used were isolated and then used for organ bath study.

CFTR genotyping

Screening of frequent CFTR mutations (50 mutations and poly-T repeats polymorphism intron 8) was performed by fluorescent ARMS (Amplification Refractory Mutation System) PCR using the kit CF-EU2v1 (Elucigene®, Manchester, UK) following the manufacturer recommendations. Amplified sequences were separated by capillary electrophoresis using an ABI PRISM 3130XL Genetic Analyzer (Applied BiosystemsTM, Foster City, CA). Data analysis and interpretation were performed with the version 5 of GeneMapper software (Applied BiosystemsTM, Foster City, CA). A sensibility > 87 % is estimated when this test is used for CFTR mutations screening in French Population [4].

***Hemodynamic measurements, and collection of tissues*-** Rats were placed under general anesthesia and spontaneous breathing with an Isoflurane Rodent Anesthesia System (Minerve, Esternay, France) (maintenance: isoflurane 2% at room air). Hemodynamic measurements such as right ventricular systolic pressure (RVSP; mmHg), cardiac output (CO; mL/min) and mean carotid pressure (mCP; mmHg) were performed prior to tissue collection, as previously described [5]. Hemodynamics values were analyzed using LabChart software. LabChart allow us to calculate several ventricular wave form parameters including; End diastolic pressure (EDP), Contractility index which correspond to Max dP/dt divided by the pressure (P) at the time of Max dP/dt.

For Fulton's index of right ventricular (RV) hypertrophy, the ratio of RV weight to left ventricular (LV) plus septal (S) weight (RV/LV+S) was calculated.

***Echocardiographic measurement*-** Evaluation by Trans-thoracic echocardiography (TTE) was performed with a digital ultrasound system (Vivid E9, GE Healthcare) by using a high-frequency phased array transducer (12 S-D 4-12MHz, GE Healthcare). Echocardiographic evaluation procedure was performed under general anesthesia and spontaneous breathing with an Isoflurane Rodent Anesthesia System (Minerve, Esternay, France) (maintenance: isoflurane 2% at room air). Rats were shaved and body temperature was controlled during experiments. All analyses were performed in a blinded fashion way: experimental conditions were unknown by the operator during TTE examination and data interpretation. Measurement of pulmonary artery acceleration time (PAAT), heart rate (HR), pulmonary artery velocity time integral (VTI), RV ejection time (RVET) velocity time integral (VTI), were performed as previously described [6, 7]. In the 4-cavity view performed in the subcostal way,

we measured RV and LV thickness, RV or LV end diastolic diameter (RV EDd, LV EDd, respectively) and systolic diameter (RV EDs, LV EDd).

Reverse transcription quantitative PCR (RT-qPCR) - Total RNA was extracted using TRIzol reagent according to standard procedures. To remove the genomic DNA contamination from the RNA preparations before reverse transcription, mRNA was treated with DNAse (Qiagen, Valencia, CA, USA; cat. no. 205311). Then, one microgram of total RNA was reverse-transcribed using a QuantiTect Reverse Transcription Kit (Qiagen, Valencia, CA, USA; cat. no. 205311). Gene expression was quantified using qPCR following the standard protocol for ready-to-use TaqMan gene expression assays (Life Technologies) on a StepOne Plus Real-Time PCR System (Life Technologies). Predesigned probe sets used for experiments were: Human *CFTR*: Hs00357011_m1, Human *β-Actin*: Hs01060665_g1 ; Rat *Cftr*: Rn01455972_m1, Rat *β-Actin*: Rn00667869_m1

Western blot analyses- Total proteins from rat lung-tissue samples were prepared as described previously[2]. All antibodies used are listed in supplemental table 3.

For CFTR protein: Human PASMC were grown and harvested using RIPA buffer (Sigma) supplemented with Protease and Phosphatase inhibitor cocktail (Roche) with EDTA. The cell lysate was sonicated and centrifuged for 10 min at 5000 g. Protein concentration of the supernatant was determined using the Pierce BCA Protein Assay Kit (Thermo Scientific), then 5 µg protein from each sample was mixed with 10x Laemmli sample buffer and ran on 8% SDS-PAGE. Followed by electrotransfer to a PVDF membrane (GE Healthcare, Little Chalfont, UK). After blocking the membrane with 5 % non-fat milk in TBS-T (5 mM Tris-Cl, 150 mM NaCl, 0.1% Tween 20, pH 7.5), the membrane was labeled for CFTR (Alomone or CF foundation) , followed by incubation with horseradish peroxidase conjugated secondary antibody. Final detection of the proteins was performed using an ECL Plus Kit (GE Healthcare, Little Chalfont, UK) and a ChemiDocTM Touch Imaging System

hPASMCs proliferation measurement- To evaluate cell proliferation, we measured BrDu incorporation to identify cell undergoing DNA replication, using a DELFIA cell proliferation kit (AD0200, PerkinElmer). Experiments were performed according to the kit recommendations. To evaluate the proliferation state of the cells, different treatment were used: CFTR inhibitor ($CFTR_{inh172}$

at 10µmol/L) or DMSO. To stimulate the cell proliferation, the medium contained 10 percent of serum.

Isometric tension measurement- Contractile responses of rat PA was measured using a small-vessel wire myograph (Danish Myotechnology, Aarhus, Denmark), as reported previously [8]. Briefly, first-order intrapulmonary arterial segments (length: 1.4–2.0 mm) were mounted on the jaws of the myograph using a 40 µm diameter tungsten wire. Data acquisition was performed using PowerLab 8/30 and LabChart® Pro v7.1 software (AD instrument).

Human and Pig PA were mounted on an emkaBATH4 modular tissue bath system (EMKA Technologie, Paris, France) coupled to IOX software (EMKA Technologie). As determined in preliminary experiments, human PA were set at optimal length by equilibration against a passive load of 0.6g.

Vessels were bathed in Krebs solution containing (in mmol/L): 119 NaCl, 4.7 KCl, 2.5 $CaCl_2$, 1.17 $MgSO_4$, 1.18 KH_2PO_4, 25 $NaHCO_3$, and 11 glucose at 37°C, and continuously aerated with a mixture of CO_2/O_2 (5%/95%). After stretching the PA at 0.9 x C_{30mmHg}, basal tone was measured as the drop of tension resulting from the replacement of Krebs bath solution with a Ca^{2+}-free solution. After adding Krebs solution again, vessels were contracted with a solution containing 100 mol/L K^+ (K100). Once a plateau was reached, the vessels were washed with Krebs solution for 30 min. DMSO or CFTRAct-A1 (C_{act}-A1) (100µmol/L) were used as pretreatments before the dose response to KCl (10-90 mmol/L) whereas MPB91 (10µmol/L to 300µmol/L) and C_{act}-A1 (1µmol/L to 200µmol/L) were used to induce relaxation after vessel contraction was obtained using thromboxane A2 analogue U46619 (1µmol/L). All modified Krebs solutions prepared with various KCl concentrations (K10 to K100) had equimolar substitution of NaCl in order to keep constant osmolarity and [Cl^-] compared to normal Krebs solution. The contractile responses were expressed relative to the response to K100 challenge. The relaxation responses were expressed as the percentage of the precontractile response obtained with U46619.

Assessment of pulmonary arterial remodeling- The wall thickness was assessed on pulmonary arteries <500µm and >100µm. Measurements were performed on 4µm thick sections of lung tissue stained with hematoxylin and eosin. Sections were examined on light microscope at 200 x

magnification. The percentage of wall thickness of muscularized arteries [(2xmedial wall thickness /external diameter) x100] was performed.

Immunofluorescence staining- Frozen lungs were prepared as described previously [9]. All antibodies used are listed in supplemental table 4.

Immunohistochemistry - Paraffin-embedded 5µm thick sections of lung samples were mounted on SuperFrostPlus slides (Thermoscientific, Villebon sur Yvette, France). The immunostainings using rabbit polyclonal antibody (CFTR 1/100 MAB25031 from R&D system) Ki67 (RBK027; Ztomed Systems) were performed according the facility automated protocol (benchmark GX autostainer, Ventana Medical System, Roche).

Correlative light and electron microscopy (CLEM) - To determine the ultrastructural localization of CFTR, correlative light and electron microscopy (CLEM) was used after immunolabelling. This approach allows pre-selection of area with features of interest for detailed ultrastructural study in transmission electron microscopy (TEM). Samples of human lung specimens (2 cm^3) were embedded and frozen after fixation in 4% paraformaldehyde and immersion in 10% then 40% sucrose solution. Indirect immunofluorescence was performed on frozen sections (10 µm) collected onto correlative microscopy coverslips® (Delta Microscopies, France). After confocal microscopy acquisition, correlative slides were detached in SPB and returned upside down. Selected thick cryo-sections were fixed 1% glutaraldehyde in SPB for 5 min at room temperature, quenched with glycine 50mM and rinsed before processing to gold amplification. One drop of gold reagent (Gold enhance EM/blot – Nanoprobes – LGF Distribution Ste Consorce – France) was applied onto sections for 10 min. After rinses, the sections were post fixed with 0.5% osmium tetroxide, gradually dehydrated in ethanol (50% to 100%) and embedded in Epon. Ultrathin sections (70 nm) were collected onto 150 mesh cooper grids, and counterstained with lead citrate before examination.

All the electron microscope examination were proceeded on Hitachi HT7700 electron microscope operated at 80 k, microphotographs were acquired with a camera AMT (Milexia, France),(MIMA2 Facility, Université Paris-Saclay, INRAE, AgroParisTech, GABI, 78350, Jouy-en-Josas, France).

After an overnight incubation at 4°C, rabbit polyclonal antibody (CFTR 1/200 MAB25031 from R&D system) was revealed by the goat anti-rabbit Alexa Fluor® 488 FluoroNanogold™ (– Nanoprobes – LGF Distribution Echirolles – France), slides were examined with a confocal microscope (LSM700; Carl Zeiss, Le Pecq, France) and images were acquired with the software Zen (Centre Chirurgical Marie Lannelongue Microscopy and Imaging Facility, Le-Plessis-Robinson, France).

Statistical analyses- All statistical tests were performed using GraphPad Prism software (GraphPad, version 6.0 for Windows). All data were verified for normal distribution using Shapiro-wilk normality test. All values are reported as mean ± S.E.M. For all experiments, the difference between two groups was assessed by T test. The difference between three groups was assessed with one-way ANOVA completed by Tukey's multiple comparisons test for post hoc analyses. Differences were considered statistically significant at p-values < 0.05.

Supplemental references

1. Ma L, Roman-Campos D, Austin ED, Eyries M, Sampson KS, Soubrier F, Germain M, Trégouët D-A, Borczuk A, Rosenzweig EB, Girerd B, Montani D, Humbert M, Loyd JE, Kass RS, Chung WK. A novel channelopathy in pulmonary arterial hypertension. *N. Engl. J. Med.* 2013; 369: 351–361.

2. Lambert M, Capuano V, Boet A, Tesson L, Bertero T, Nakhleh MK, Remy S, Anegon I, Pechoux C, Hautefort A, Rucker-Martin C, Manoury B, Domergue V, Mercier O, Girerd B, Montani D, Perros F, Humbert M, Antigny F. Characterization of Kcnk3-Mutated Rat, a Novel Model of Pulmonary Hypertension. *Circ. Res.* 2019; 125: 678–695.

3. Dreano E, Bacchetta M, Simonin J, Galmiche L, Usal C, Slimani L, Sadoine J, Tesson L, Anegon I, Concordet J-P, Hatton A, Vignaud L, Tondelier D, Sermet-Gaudelus I, Chanson M, Cottart C-H. Characterization of two rat models of cystic fibrosis-KO and F508del CFTR-Generated by Crispr-Cas9. *Animal Model Exp Med* 2019; 2: 297–311.

4. Audrézet MP, Munck A, Scotet V, Claustres M, Roussey M, Delmas D, Férec C, Desgeorges M. Comprehensive CFTR gene analysis of the French cystic fibrosis screened newborn cohort: implications for diagnosis, genetic counseling, and mutation-specific therapy. *Genet. Med.* 2015; 17: 108–116.

5. Perros F, Günther S, Ranchoux B, Godinas L, Antigny F, Chaumais M-C, Dorfmüller P, Hautefort A, Raymond N, Savale L, Jaïs X, Girerd B, Cottin V, Sitbon O, Simonneau G, Humbert M, Montani D. Mitomycin-Induced Pulmonary Veno-Occlusive DiseaseCLINICAL PERSPECTIVE: Evidence From Human Disease and Animal Models. *Circulation* 2015; 132: 834–847.

6. Sabourin J, Boet A, Rucker-Martin C, Lambert M, Gomez A-M, Benitah J-P, Perros F, Humbert M, Antigny F. Ca2+ handling remodeling and STIM1L/Orai1/TRPC1/TRPC4 upregulation in monocrotaline-induced right ventricular hypertrophy. *J. Mol. Cell. Cardiol.* 2018; 118: 208–224.

7. Lambert M, Boet A, Rucker-Martin C, Mendes-Ferreira P, Capuano V, Hatem S, Adão R, Brás-Silva C, Hautefort A, Michel J-B, Dorfmuller P, Fadel E, Kotsimbos T, Price L, Jourdon P, Montani D, Humbert M, Perros F, Antigny F. Loss of KCNK3 is a hallmark of RV hypertrophy/dysfunction associated with pulmonary hypertension. *Cardiovasc. Res.* 2018; .

8. Hautefort A, Mendes-Ferreira P, Sabourin J, Manaud G, Bertero T, Rucker-Martin C, Riou M, Adão R, Manoury B, Lambert M, Boet A, Lecerf F, Domergue V, Brás-Silva C, Gomez AM, Montani D, Girerd B, Humbert M, Antigny F, Perros F. Bmpr2 Mutant Rats Develop Pulmonary and Cardiac Characteristics of Pulmonary Arterial Hypertension. *Circulation* 2019; 139: 932–948.

9. Antigny F, Hautefort A, Meloche J, Belacel-Ouari M, Manoury B, Rucker-Martin C, Péchoux C, Potus F, Nadeau V, Tremblay E, Ruffenach G, Bourgeois A, Dorfmüller P, Breuils-Bonnet S, Fadel E, Ranchoux B, Jourdon P, Girerd B, Montani D, Provencher S, Bonnet S, Simonneau G, Humbert M, Perros F. Potassium Channel Subfamily K Member 3 (KCNK3) Contributes to the Development of Pulmonary Arterial Hypertension. *Circulation* 2016; 133: 1371–1385.

Supplemental tables

Supplemental table 1. List of 51 most common mutation in *CFTR* analyzed in iPAH patients

	CFTR NM_000492.3		
Mutations	**c.* HGVS nomenclature**	**p.* HGVS nomenclature**	**Frequency**
CFTRdele2,3	c.54-5940_273+1025deI21kb		
E6OX	c.178G>T	p.(G1u60*)	0.17%
P67L	c.200C>T	p.(Pro67Leu)	
G85E	c.254G>A	p.(Gly85G1u)	0.34%
394deITT	c.262_263deITT	p.(Leu88Ilefs*22)	0.17%
444delA	c.313de1A	p.(Ile105Serfs*2)	
R117C	c.349C>T	p.(Arg117Cys)	
R117H	c.350G>A	p.(Arg117His)	0.3%
Y122X	c.366T>A	p.(Tyr122*)	0.97%
621+1G>T	c.489+1G>T		0.26%
711+1G>T	c.579+1G>T		0.67%
L206W	c.617T>G	p.{Leu206Trp)	
1078delT	c.948de1T	p.(Phe316Leufs*12)	0.22%
R334W	c.1000C>T	p.(Arg334Trp)	0.3%
R347P	c.1040G>C	p.(Arg347Pro)	0.56%
R347H	c.1040G>A	p.(Arg347His)	
A455E	c.1364C>A	p.{Ala455G1u)	0.22%
1507de1	c.1519_1521delATC	p.(Ile507del)	0.63%
F508de1	c.1521_1523deICTT	p.{Phe508del)	67.24%
1677delTA	c.1545_1546delTA	p.(Tyr515*)	
V520F	c.1558G>T	p.(Va1520Phe)	
1717-1G>A	c.1585-1G>A		1.47%
G542X	c.1624G>T	p.(Gly542*)	3.19%
S549R(T>G)	c.1647T>G	p.(Ser549Arg)	
S549N	c.1646G>A	p.(Ser549Asn)	
G551D	c.1652G>A	p.(Gly551Asp)	1.16%
R553X	c.1657C>T	p.(Arg553*)	1.29%
R560T	c.1679G>C	p.(Arg560Thr)	
1811+1.6kbA>G	c.1679+1.6kbA>G		0.39%
1898+1G>A	c.1766+1G>A		
2143de1T	c.2010de1T	p.(1eu671*)	
2183AA>G	c.2051_2052delinsG		
2184delA	c.2052de1A	p.(Lys684Asnfs*38)	
2347deIG	c.2215deIG	p.(Va1739Tyrfs*16)	
W846X	c.2538G>A	p.(Trp846*)	0.26%
2789+5G>A	c.2657+5G>A		1.42%
Q890X	c.2668C>T	p.(G1n890*)	
3120+1G>A	c.2988+1G>A		0.82%
3272-26A>G	c.3140-26A>G		0.59%
R1066C	c.3196C>T	p.(Arg1066Cys)	
Y1092X(C>A)	c.3276C>A	p.(Tyr1092*)	0.48%
M1101K	c.3302T>A	p.(Met1101Lys)	
D1152H	c.3454G>C	p.(Asp1152His)	
R1158X	c.3472C>T	p.(Arg1158*)	
R1162X	c.3484C>T	p.(Arg1162*)	0.56%
3659deIC	c.3528deIC	p.(Lys1177fs)	0.41%
3849+10kbC>T	c.3717+10kbC>T		0.13%
S1251N	c.3752G>A	p.(Ser1251Asn)	0.3%
3905insT	c.3773dupT	p.(Leu1258fs)	
W1282X	c.3846G>A	p.(Trp1282*)	0.52%
N1303K	c.3909C>G	p.(Asn1303Lys)	1.98%

Supplemental table 2: Echocardiographic parameters measured in DMSO- or $CFTR_{inh172}$-treated rats (n=9 rats). *p<0.05, **p<0.01, ***p<0.001 vs. DMSO. Experiments were analyzed using the Mann-Whitney test.

	DMSO (n=9)	**$CFTR_{inh172}$ (n=9)**
HR (bpm)	435.9 ± 7.4	442.4 ± 15.1
PAAT (ms)	36.3 ± 0.9	26.1 ± 1.2 **
ITV pulmonary artery (mm)	5.82 ± 0.38	5.06 ± 0.32
PAAT/RVET	0.47 ± 0.018	0.37 ± 0.017 **
RV thickness (mm)	1.1 ± 0.06	1.027 ± 0.058
ITV aorta (mm)	6 ± 0.23	6.4 ± 0.2
LV thickness (mm)	1.24 ± 0.07	1.4 ± 0.09

Supplemental table 3: Characteristics of primary antibodies used in western blot studies

ANTIBODY	SPECIES	DILUTION	SUPLIER	REFERENCE
CFTR	Mouse	1/1000	Alomone Labs	ACL-006
p-ERK 1/2	Rabbit	1/1000	Cell signaling	9102
p-P38	Rabbit	1/1000	Cell signaling	9211S
p-akt (Thr308)	Rabbit	1/1000	Cell signaling	9275
CD45	Rabbit	1/1000	BD Biosciences	610266
Ve-Cadherin	Rabbit	1/1000	Abcam	Ab331
Serum albumin	Rabbit	1/1000	R&D Systems	MAB1455
β-Actin	Mouse	1/5000	Sigma	A1978
CFTR	Rabbit	1/1000	Alomone	ACL-006
CFTR	Mouse	1/1000	CF foundation	#596

Supplemental table 4: Characteristics of primary antibodies used in immunofluorescence studies

ANTIBODY	SPECIES	DILUTION	SUPLIER	REFERENCE
α-SMA-FITC	Mouse	1/200	Sigma-Aldritch	F3777
VWF	Rabbit	1/300	Dako	A0082
CFTR	Rabbit	1/200	R&D Systems	MAB25031

Supplemental figures

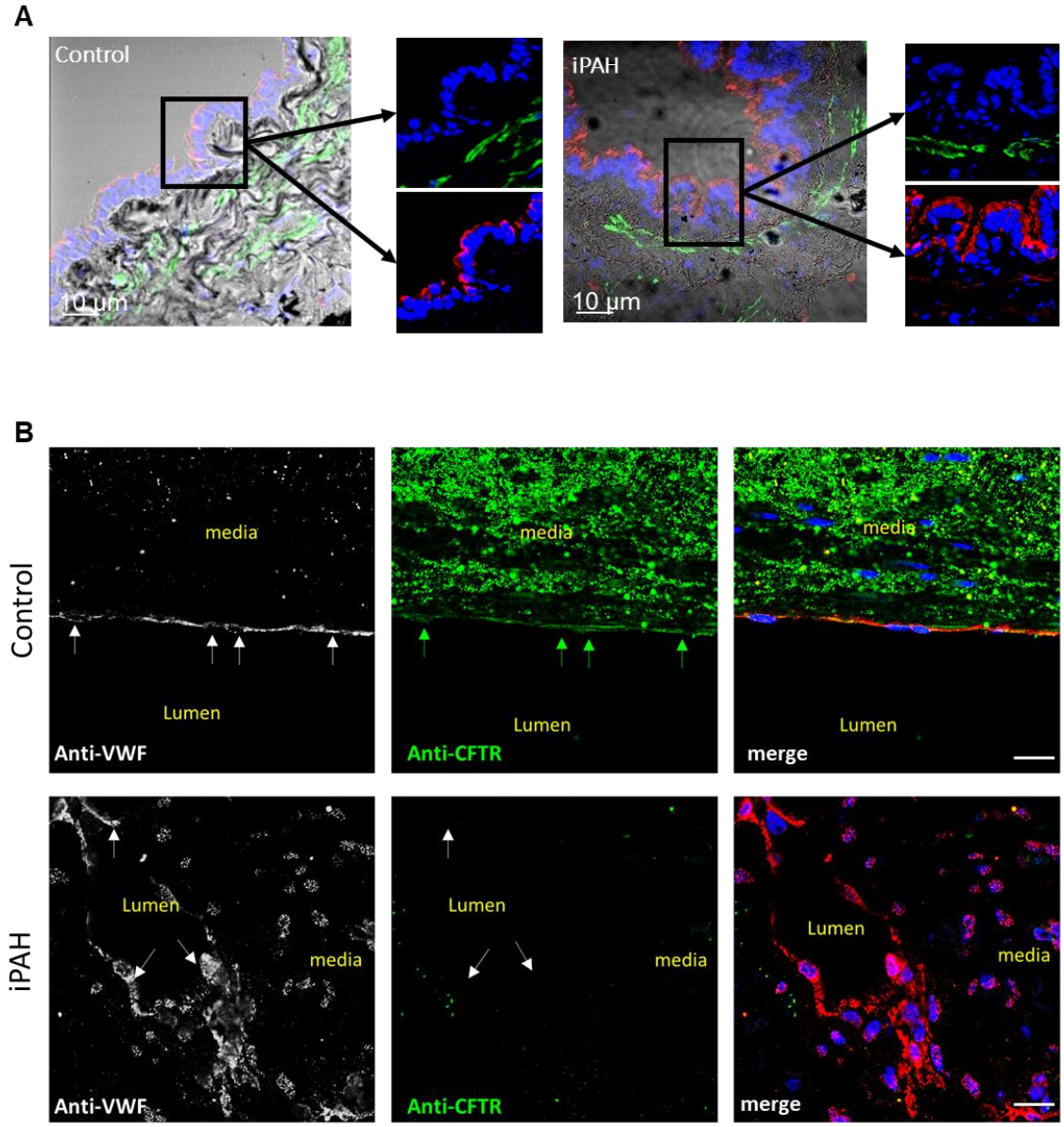

Supplemental Figure 1

Supplemental Figure 1: CFTR expression lung from iPAH. (A) Immunofluorescence labeling and confocal imaging of bronchia from non PAH and idiopathic PAH (iPAH) patients lungs, through α-SMA (green) and CFTR (red), and DAPI in blue. (B) Immunofluorescence labeling and confocal

imaging of pulmonary artery from non PAH and idiopathic PAH (iPAH) patients lungs, through Von Willebrand factor (VWF) (white), CFTR (green) and DAPI in blue, Bar graph = 10µm.

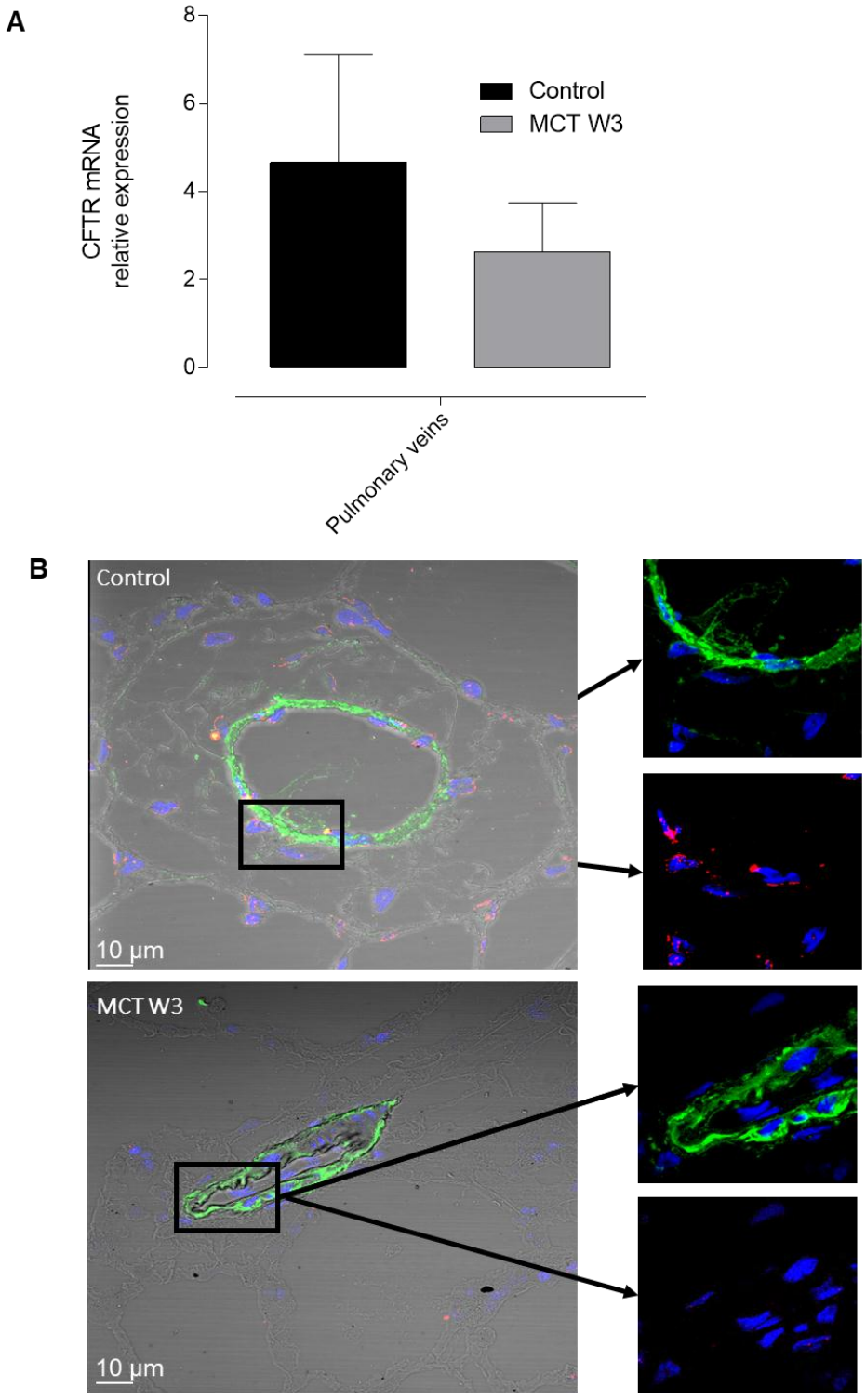

Supplemental Figure 2

Supplemental Figure 2: CFTR expression lung from MCT-PH rats. (A) mRNA level expression of *CFTR* on pulmonary veins isolated from control and MCT-PH (week 3) rats (n=4 for each group). (B) Immunofluorescence labeling and confocal imaging of Rat PA from control and MCT-PH lungs (at 3 weeks after MCT injection), through α-SMA (green) and CFTR (red).

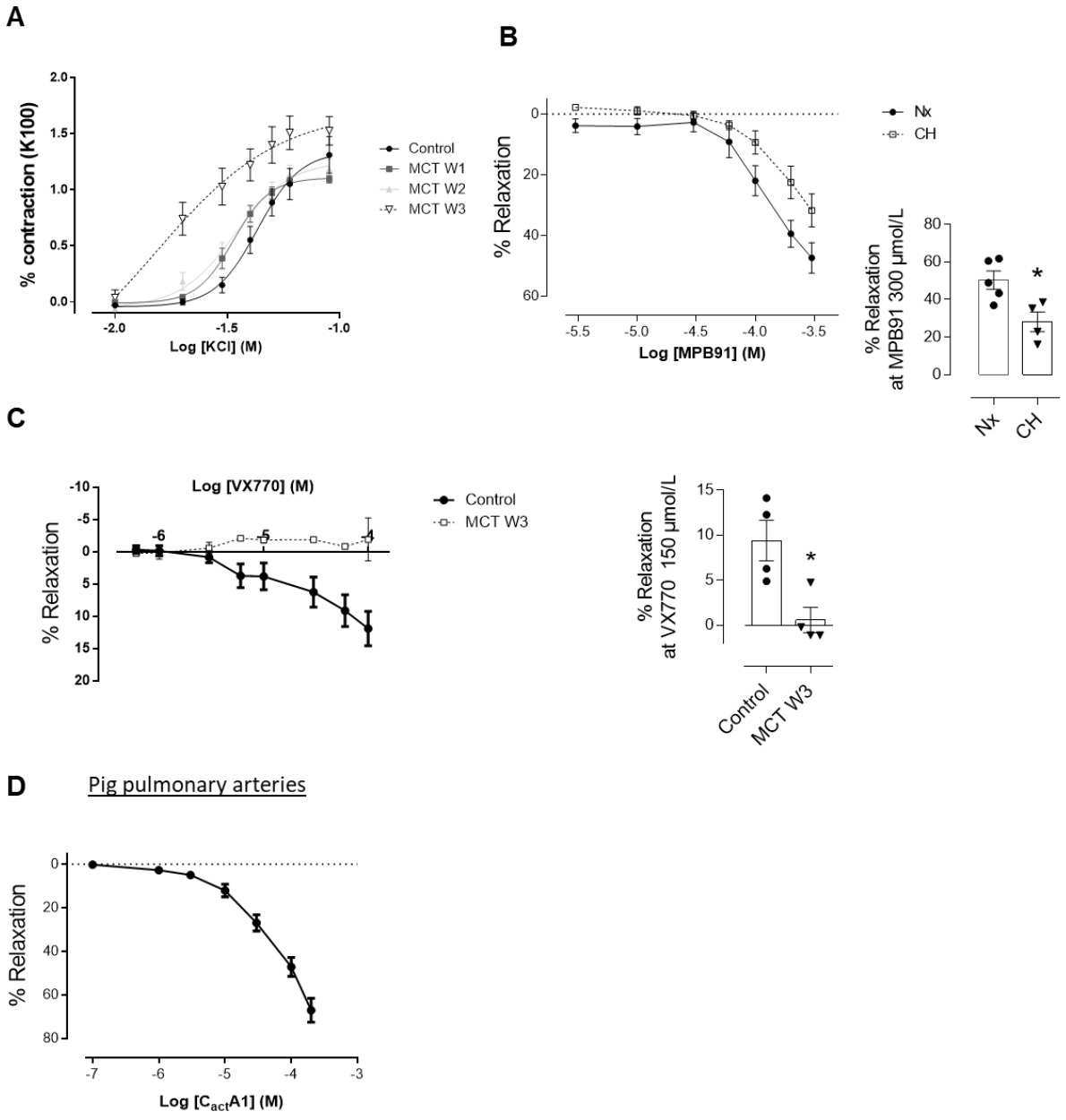

Supplemental Figure 3

Supplemental figure 3: (A) Concentration-response curve (normalized to K100) established by applying increasing concentrations of K^+ on PA isolated from control rats and MCT-exposed rats (at

week 1, week 2 and week 3). (B) Relaxant response to cumulative concentrations of CFTR activator MPB91 (MPB91; 1 µmol/L to 300 µmol/L) in PA segments isolated from rats exposed to normoxia (Nx) or chronic hypoxia (CH, 3 weeks). Right panel, corresponding graph of the percent of relaxation to 300 µmol/L MPB91 (n=5–8rats). (C) Relaxant response to cumulative concentrations of the CFTR potentiator VX770 in PA segments isolated from control and MCT-exposed rats (3 weeks) (n=4 rats). (D) Relaxant response to cumulative concentrations of $C_{act}A1$ ($C_{act}A1$, 1 µmol/L to 200 µmol/L) in PA segments isolated from healthy pigs (n=5 pigs). ns:non-significant. *$p< 0.05$ *vs. Control*. Data were analyzed using Mann-Whitney test.

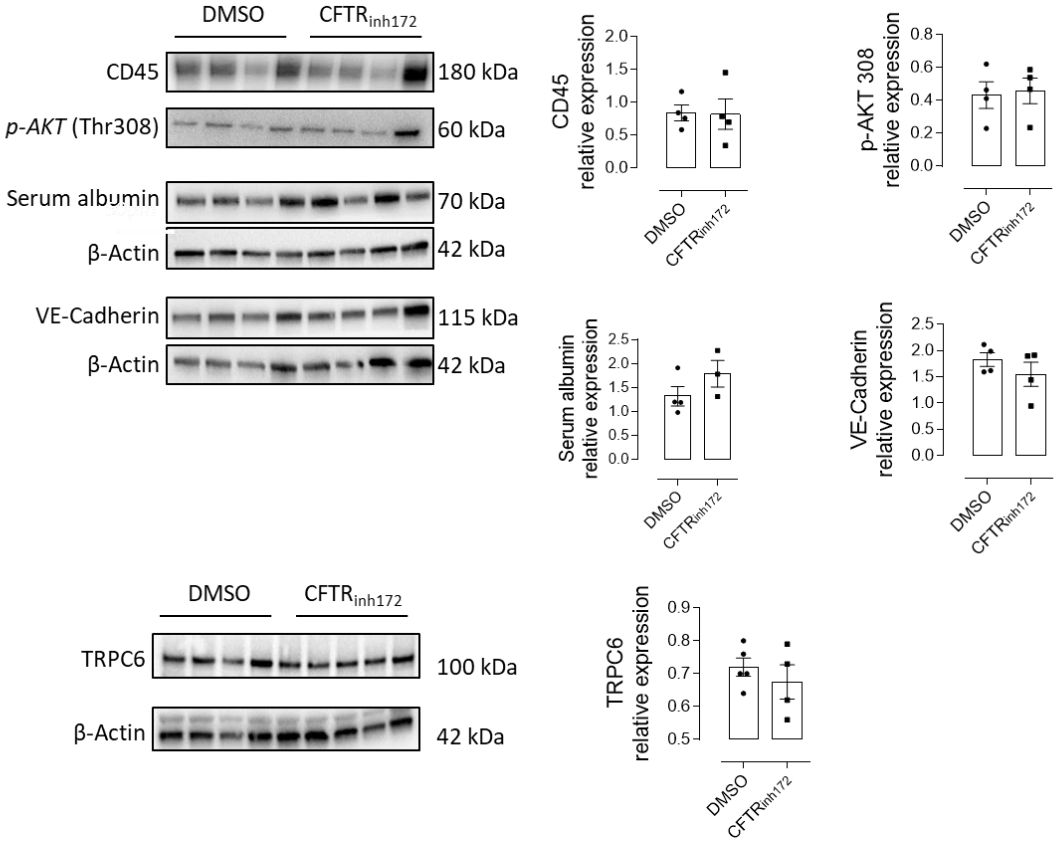

Supplemental Figure 4

Supplemental Figure 4: Representative western blots and quantification of CD45, p-308AKT, VE cadherin, serum albumin and TRPC6 expression in lungs from DMSO and $CFTR_{inh}$-172 treated rats (n=4 rats).

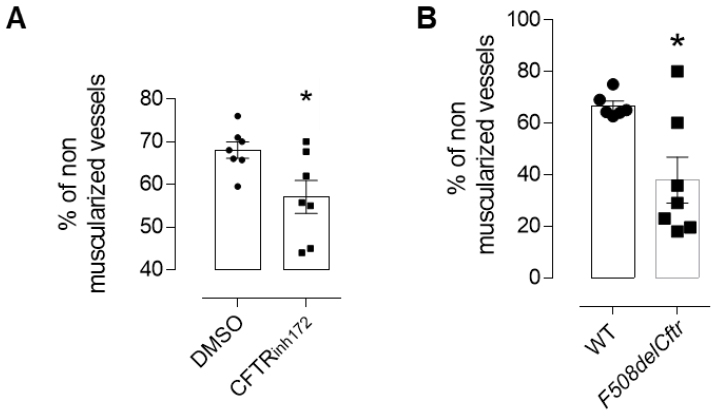

Supplemental Figure 5

Supplemental figure 5: Percentage of non muscularized vessels in lung from $CFTR_{inh}$172-exposed rats and *F508delCftr* rats. (A) Percentage of non muscularized vessels (100 vessels count per rat, n=7 rats) in DMSO or $CFTR_{inh172}$-exposed rats as measured by immunostaining against α-smooth-muscle actin (αSMA) and Von Willebrand Factor (VWF). (B) Percentage of non muscularized vessels (100 vessels count per rat, n=7 rats) in WT and *F508delCftr* rats as measured by immunostaining against α-smooth-muscle actin (αSMA) and Von Willebrand Factor (VWF).

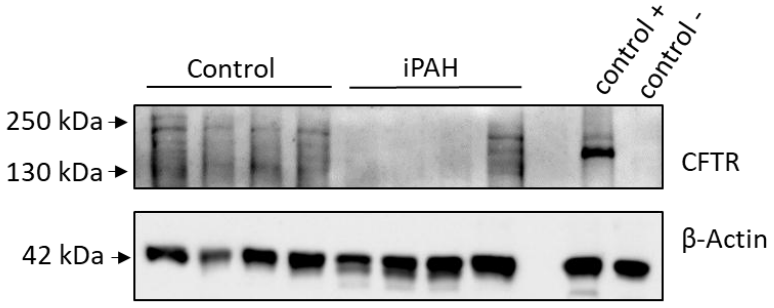

Supplemental Figure 6

Supplemental Figure 6: CFTR protein expression in hPASMCs from control and iPAH patients. Representative western blots and quantification of CFTR in hPASMCs from control (n=4), iPAH patients (n=4), human lung (positive control) and human adenocarcinomic alveolar basal epithelial cells cells (A549 cells) (negative control).

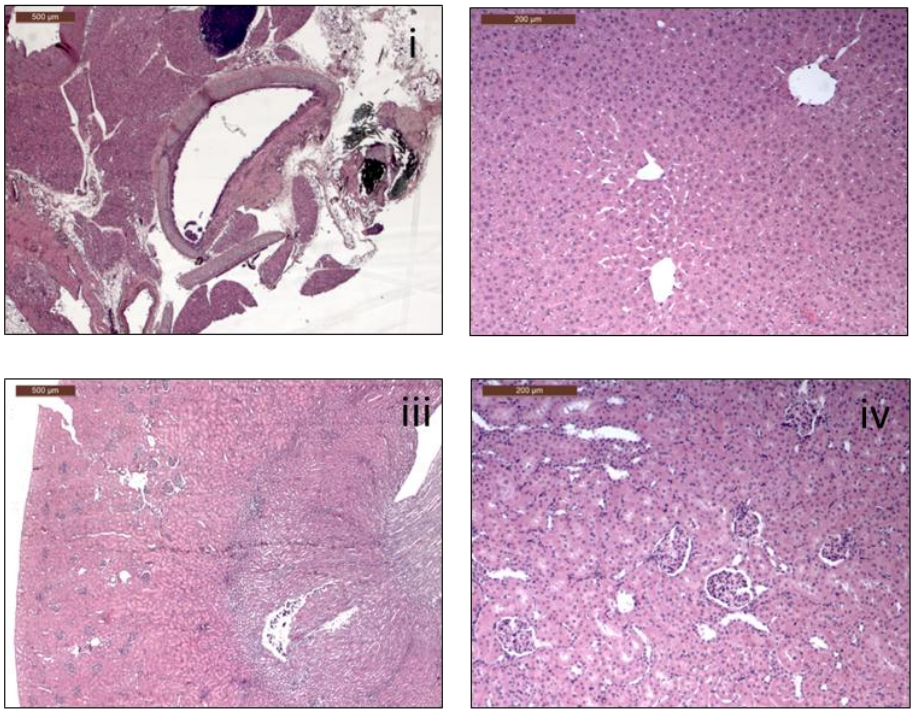

Supplemental Figure 7

Supplemental Figure 7: Pathological assessment of the bronchial tree, liver and kidney from $CFTR_{inh}$172-exposed rats. i) Mediastinal tissue cross section, incorporating brown fat and trachea. Cartilage rings are well structured as well as mucosa and submucosa. No inflammation is observed. ii) Liver tissue is devoid of major pathological alteration. Only mild dilation of centro-lobular capillaries is visible. iii) Kidney histology with view of cortical and medullary tissue. Renal cortex contains well-formed glomeruli, without significant fibrous involution (iv).